Research Article

The Journal of Comparative Neurology
Research in Systems Neuroscience
DOI 10.1002/cne.23227

Afferent Regulation of Chicken Auditory Brainstem Neurons: Rapid Changes in Phosphorylation of Elongation Factor 2

Ethan G. McBride, Edwin W Rubel, and Yuan Wang

Virginia Merrill Bloedel Hearing Research Center, Department of Otolaryngology-Head and Neck Surgery, Department of Physiology and Biophysics, University of Washington School of Medicine, Box 357923, Seattle, WA 98195, USA

Abbreviated title: eEF2 in afferent regulation of neuron survival

Associate Editor: Oswald Steward, University of California–Irvine

Correspondence to: Yuan Wang

Department of Otolaryngology

Mail Stop 357923, University of Washington

Seattle, WA 98195

Phone: (206) 616-4113; Fax: (206) 616-1828

email: wangyuan@uw.edu

Key Words: apoptosis; cell death; protein synthesis; cochlea removal; afferent deprivation; nucleus magnocellularis

Acknowledgements: Sponsored by National Institute on Deafness and Other Communication Disorders grants DC-03829, DC-02739, DC-04661, and DC-00018; Deafness Research Foundation research grant; and the University of Washington Mary Gates Endowment scholarship

This article has been accepted for publication and undergone full peer review but has not been through the copyediting, typesetting, pagination and proofreading process which may lead to differences between this version and the Version of Record. Please cite this article as an 'Accepted Article', doi: 10.1002/cne.23227
© 2012 Wiley Periodicals, Inc.
Received: Jun 27, 2012; Revised: Sep 05, 2012; Accepted: Sep 07, 2012

Accepted Article

Abstract

The relationships between protein synthesis and neuronal survival are poorly understood. In chicken nucleus magnocellularis (NM), significant alterations in overall protein synthesis precede neuronal death induced by deprivation of excitatory afferent activity. Previously we demonstrated an initial reduction in the overall rate of protein synthesis in all deprived NM neurons, followed by quick recovery (starting at 6h) in some, but not all, neurons. Neurons with recovered protein synthesis ultimately survive while others become "ghost" cells (no detectable Nissl substance) at 12-24h and die within 48h. To explore the mechanisms underlying this differential influence of afferent input on protein synthesis and cell survival, the current study investigates the involvement of eukaryotic translation elongation factor 2 (eEF2), the phosphorylation of which reduces overall protein synthesis. Using immunocytochemistry for either total or phosphorylated eEF2 (p-eEF2), we find significant reductions in the level of phosphorylated, but not total, eEF2 in NM neurons as early as 0.5h to 1h following cochlea removal. Unexpectedly, neurons with low levels of p-eEF2 show reduced protein synthesis at 6h indicated by a marker for active ribosomes. At 12h, all "ghost" cells exhibited little or no p-eEF2 staining although not every neuron with a comparable low level of p-eEF2 was a "ghost" cell. These observations demonstrate that a reduced level of p-eEF2 is not responsible for immediate responses (including reduced overall protein synthesis) of a neuron to compromised afferent input, but may impair the neuron's ability to initiate recovery signaling for survival and make the neuron more vulnerable to death.

Accepted Article

Introduction

The importance of afferent input to neural integrity has been well demonstrated in many systems (Guillery, 1973; Kalil, 1980; Trune, 1982; Clarke and Egloff, 1988; Rubel and Fritzsch, 2002; Vankirk and Byrd, 2003). Neuronal cell death induced by afferent deprivation involves significant alterations in the overall rate of protein synthesis, as well as in the expression level of certain apoptotic and anti-apoptotic proteins (Steward and Rubel, 1985; Garden et al., 1994; Mostafapour et al., 2000, 2002; Wilkinson et al., 2002, 2003; Robinson et al., 2003; Karnes et al., 2009). However, it is not fully understood how overall protein synthesis and translation of specific proteins are regulated by afferent inputs and how this regulation influences cell survival.

One important way that protein synthesis is regulated is through phosphorylation-induced modulation of the activity of eukaryotic translation elongation factor 2 (eEF2). eEF2 catalyzes changes in ribosome conformation for elongation of the amino acid chain during the elongation phase of protein translation (Nairn and Palfrey, 1987; Jørgensen et al., 2006; Kaul et al., 2011). When phosphorylated, eEF2 loses its affinity for the ribosome, slowing or stopping translation and overall protein synthesis (Ryazanov et al., 1988; Carlberg et al., 1990; Redpath et al., 1993). In non-neuronal cells, the resulting suppression of translation leads to reduced cell viability and apoptosis (White-Gilbertson et al., 2008) or serves to conserve energy under starvation (Kaul et al., 2011). In addition, eEF2 phosphorylation *promotes* the translation of a number of selected proteins, including the anti-apoptotic protein Bcl-xL (Zhang et al., 2011). A high level of phosphorylated eEF2 (p-eEF2) and associated Bcl-xL synthesis are critical for the growth, survival, and proliferation of cancer cells (Bagaglio et al., 1993; Cheng et al., 1995; Parmer et al., 1999; Arora et al., 2003; Wu et al., 2006; Nakamura et al., 2009; Chen et al., 2011; Zhang et al., 2011).

Accepted Article

The role of eEF2 phosphorylation-mediated protein synthesis in *neuronal* cell survival, however, has been considerably less well-studied. Although tight regulation of eEF2 phosphorylation by sensory input and glutamate neurotransmission has been documented extensively (Marin et al., 1997; Scheetz et al., 1997, 2000; Chotiner et al., 2003; Sutton et al., 2007, 2004, 2006; Lenz and Avruch, 2005; Cossenza et al., 2006; Nosyreva and Kavalali, 2010; Autry et al., 2011), this regulation is mostly studied for its involvement in local dendritic protein translation and activity-dependent synaptic plasticity (Scheetz et al., 2000; Park et al., 2008; Verpelli et al., 2010). In contrast, whether and how eEF2 activity affects the survival of a neuron after a variety of challenges remains mostly unknown. One exception is a study in cultured cortical neurons in which eEF2 phosphorylation induced suppression in overall protein translation, apparently protecting neurons from glutamate excitotoxicity (Marin et al., 1997).

Here we identify a novel relationship among eEF2 phosphorylation, overall protein synthesis, and afferent-regulated cell survival and/or death in chicken brainstem auditory pathways. In birds, nucleus magnocellularis (NM) contains a homogeneous population of neurons that are comparable to bushy neurons in the mammalian anteroventral cochlear nucleus (AVCN). NM and AVCN neurons receive excitatory input from the ipsilateral auditory nerve. Deprivation of this excitatory input by removal of the cochlea induces age-dependent cell death in both nuclei (Born and Rubel, 1985; Hashisaki and Rubel, 1989; Moore, 1990; Tierney et al., 1997; Rubel and Fritzsch, 2002; Mostafapour et al., 2000, 2002). In NM, the time course of cellular changes resulting in cell death or survival has been studied in detail: a subpopulation of neurons dies quickly within 2 days while others survive (Born and Rubel, 1985). Thus NM provides an excellent model for identifying critical signaling required in neuronal survival by addressing the question of why some neurons die and others survive under the same challenge.

Accepted Article

Previous studies have demonstrated that the overall rate of protein synthesis is a reliable indicator of the fate of individual neurons following afferent deprivation. Shortly after cochlea removal, all deprived NM neurons exhibit reduced overall protein synthesis (Steward and Rubel, 1985; Born and Rubel, 1988) and metabolic activity (Heil and Scheich, 1986; Born et al., 1991). Six hours later, approximately 70% of deprived neurons begin to recover synthetic and metabolic activity and ultimately survive, while the remaining 30% continue with low levels of synthetic activity and die within two days following polyribosome degradation and mitochondrial vacuolization (Born and Rubel, 1985; Steward and Rubel, 1985; Garden et al., 1994, 1995 a; b). Thus, a persistent reduction in the overall rate of protein synthesis marks cell death following afferent deprivation. Two remaining questions are how afferent deprivation leads to the initial reduction in protein synthesis and why the later recovery takes place in some but not all neurons.

Using immunocytochemistry, the current study demonstrates rapid reductions in the level of phosphorylated, but not total, eEF2 in NM neurons following ipsilateral cochlea removal. Many neurons with low levels of p-eEF2 are not able to recover adequate protein synthesis levels and eventually die, demonstrating a robust relationship between the level of p-eEF2 and neuron survival following afferent deprivation. Given that eEF2 phosphorylation reduces overall protein synthesis, we suggest that the observed reduction in the level of p-eEF2 is not directly related to the early reduction in overall protein synthesis of deprived NM neurons, but may contribute to a failure in initiating or upregulating recovery/survival pathways in challenged neurons.

Materials and Methods

Fifty-seven (57) white leghorn chicken hatchlings of 4-10 days old were used for this study. Eggs were obtained from Featherland Farms (Eugene, OR) and incubated and hatched at a University of

Accepted Article

Washington vivarium. All procedures were approved by the University of Washington Institutional Animal Care and Use Committee and carried out in accordance with the National Institutes of Health Guide for the Care and Use of Laboratory Animals. All efforts were made to minimize pain and discomfort of the animals and to minimize the number of animals used.

Cochlea removal

Deprivation of excitatory afferent input to NM neurons on the right side of the brain was produced by removal of the right basilar papilla (the avian cochlea). Excitatory afferent input to the left NM remained intact so that NM neurons on the left side of the brain served as a within-animal control. The surgical procedure was described previously (Born and Rubel, 1985). Briefly, animals were anesthetized with a mixture of 40 mg/kg ketamine and 12 mg/kg xylazine. A small incision was made to widen the external ear canal. The tympanic membrane and middle ear ossicle were removed and the cochlea was pulled out through the round window. The removed cochlea was floated on water and examined with a dissecting microscope to verify complete removal. Only animals with a complete removal of the right cochlea were used for further tissue processing and data analyses. Animals were allowed to survive 0.5 (n=7), 1 (n=9), 3 (n=7), 6 (n=11), 12 (n=9), or 48 hours (n=4). An additional 10 unoperated animals were used as controls.

Antibody characterization

Four primary antibodies were used for immunocytochemistry. To avoid staining saturation and to ensure the ability of detecting bidirectional changes in staining optical density, the optimal concentration for each antibody was determined by testing a series of dilutions ranging from 1:500 to 1:50. Immunogen, host species, clone type, manufacturer's information, as well as dilution used for each antibody, are listed in Table 1.

Accepted Article

Anti-eEF2 detects endogenous levels of total eEF2 independent of phosphorylation. According to the data sheet from the manufacturer, this antibody is predicted to recognize chicken eEF2 at 95 kDa based on 100% sequence homology with human and mouse eEF2. We confirmed this by performing a western blot on chicken brainstem tissue. The anti-eEF2 antibody recognized a single band with the appropriate molecular weight (Fig. 1B). In addition, this antibody detects a band of ~95 kDa in HEK293 cells with or without treatment of phosphatase, which dephosphorylates eEF2 (Fig. 1A).

Anti-p-eEF2 detects endogenous levels of eEF2 only when phosphorylated at Thr56. It does not recognize eEF2 phosphorylated at other sites, however eEF2 cannot be phosphorylated at its other phosphorylation site, Thr58, without first being phosphorylated at Thr56, and double-phosphorylated eEF2 has nearly identical activity to single-phosphorylated eEF2 (Redpath et al., 1993). According to the data sheet from the manufacturer, this anti-p-eEF2 antibody recognizes chicken p-eEF2 at 95 kDa, which we confirmed by performing a western blot on chicken brainstem tissue. The anti-p-eEF2 antibody recognized a single band with the appropriate molecular weight (Fig. 1B). In addition, this antibody detects a band of ~95 kDa in HEK293 cells in normal buffer. This band is absent in HEK293 cells treated with phosphatase (Fig. 1A).

The Y10B antibody for ribosomal RNA (rRNA) was obtained from pooled supernatant collected from the Y10B hybridoma that was originally provided by Dr. Joan Steitz at Yale University. The production of the antibody was described previously (Lerner et al., 1981). The Y10B antibody immunoprecipitates whole ribosomes as well as all sizes of phenol-extracted rRNA, indicating that it recognizes a nucleic acid motif common to many rRNAs (Lerner et al., 1981; Garden et al., 1994). This antibody has been used extensively in previous studies in the chicken auditory brainstem nucleus as a marker for active ribosomes and overall protein synthesis (Garden et al., 1995 a; b, 1994; Hyson

and Rubel, 1995; Kim et al., 2005). The staining pattern in the current study is comparable to that reported previously.

Anti-microtubule associated protein 2 (anti-MAP2) detects endogenous levels of MAP2a and MAP2b protein, a neuronal marker that associates with microtubules, neurofilaments, and actin filaments. According to the manufacturer's data sheet, anti-MAP2 recognizes chicken MAP-2 as a 300kD band in western blot analysis. This antibody has been used as a somatodendritic marker in the chicken brain (Yamaguchi et al., 2008, 2011) and more specifically, in chicken auditory brainstem nuclei including NM (Wang and Rubel, 2008; Wang et al., 2009). The staining pattern in the current study is comparable to that reported in these studies.

Western blot

A western blot immunoassay was conducted to confirm the specificity of anti-eEF2 and anti-p-eEF2 used in the present study. For phosphatase treatment, HEK293 cells were incubated in a lysis buffer with Calf Intestinal Phosphatase (CIP; # M0290S; New England Biolabs, Ipswich, MA) at 1 unit CIP per 1 µg protein for 30 minutes at 37ºC before harvest. Brain protein samples were harvested from the NM and the surrounding region in the dorsocaudal brainstem of chicks. Molecular weight standards were used to determine relative sizes of labeled proteins. The western blot procedure for this tissue was described previously (Wang et al., 2009). Briefly, all samples were homogenized in lysis buffer with protease inhibitor cocktail (# P8340; Sigma, St. Louis, MO). Each sample (5 µg protein) was boiled for 5 minutes to denature protein and loaded onto a 4 -20% SDS-polyacrylamide gel (Bio-Rad, Hercules, CA). The gel was run for 100 minutes at 100 V. Protein was then electroblotted to a PVDF membrane (Bio-Rad). Membranes were blocked in 5% nonfat milk and probed with the antibodies (1:1,000). Horseradish peroxidase (HRP)-conjugated secondary antibodies (1:3,000; Bio-Rad) were used for detection with enhanced chemiluminescent reagents (ECL; Amersham, Little Chalfont,

Accepted Article

Buckinghamshire, England). An antibody against β-actin (Abcam Inc., Cambridge, MA) was used as a protein loading control.

Immunocytochemistry

Following the surgery and designated survival periods, animals were deeply anesthetized and transcardially perfused with phosphate-buffered saline (PBS; 0.01M) followed by 4% paraformaldehyde in 0.1M phosphate buffer. Brains were removed from the skull, postfixed overnight, and cryoprotected in 15% and 30% sucrose in PBS. The brains were then frozen with dry ice and sliced coronally at 30 μm on a sledge freezing microtome. Alternate consecutive sections were collected in PBS and labeled by single or double immunocytochemistry.

For single immunocytochemistry for eEF2 or p-eEF2, free-floating sections were incubated in a primary antibody solution with normal goat serum (1:200) at 4ºC overnight. This was followed by incubation with biotinylated goat anti-rabbit IgG antibody (1:400; Vector Laboratories, Burlingame, CA) at 4ºC overnight. Sections were then incubated in avidin-biotin-peroxidase complex solution (1:100; ABC Elite kit; Vector Laboratories) for 1 hour at room temperature. Immunoreactivity was visualized by incubating sections for 6-10 minutes in 0.045% 3-3-diaminobenzidine (Sigma) with 0.03% hydrogen peroxide. Sections were mounted on glass slides, then dehydrated, cleared, and coverslipped with DPX mounting medium (EMS, Hatfield, PA).

For double immunocytochemistry, following primary antibody incubation sections were incubated with fluorescent secondary antibodies, Alexa 488 goat anti-rabbit and Alexa 568 goat anti-mouse (1:200; # A11008 and # A11004, respectively, Invitrogen Molecular Probes, Eugene, OR), for 2 hours at room temperature. For double labeling of p-eEF2 immunoreactivity and Nissl substance, sections were first immunolabeled for p-eEF2 using Alexa 488 goat anti-rabbit secondary antibody and then incubated in Neurotrace deep red, a fluorescent marker for Nissl substance (1:75; # N-21483,

Accepted Article

Accepted Article

Invitrogen Molecular Probes), for 1 hour. Fluorescently labeled sections were then mounted on glass slides and coverslipped with Fluoromount (# 0100-01, Southern Biotech, Birmingham, AL).

Quantification of changes in eEF2 and p-eEF2 immunoreactivities

All measurements were conducted from sections labeled with single immunocytochemistry. Four to eight animals were used for each survival group and each antibody. For each animal, three sections were chosen: one each from the caudal, intermediate, and rostral regions of NM, as close as possible to the 25, 50, and 75% positions in the caudal-rostral axis of the nucleus, respectively. For each section, NM neurons on each side of the brain were imaged using brightfield optics with a 63x lens on a Zeiss Axioplan microscope. For areas containing lightly labeled neurons, an additional image was captured using differential interference contrast to help identify cell and nuclear boundaries. Neurons whose boundaries could not be unambiguously identified or those that did not contain a well-defined nucleus in the images were excluded from analyses. For each included neuron, the mean gray value of the cytoplasm (the nucleus was excluded) was measured using ImageJ software (National Institutes of Health, Bethesda, MD) and converted to optical density using a step tablet. No further image adjustments were conducted except for the images used for illustration.

To allow quantified comparison between sides and survival groups, the optical density of each neuron was normalized to generate a *z-score* using a method that has been used extensively to quantify changes in staining intensities at the individual cell level (Born and Rubel, 1988; Garden et al., 1994, 1995 a; b; Hyson and Rubel, 1995; Karnes et al., 2010). Briefly, for each section, the mean and standard deviation of the optical density were calculated across all measured neurons in the left (intact) NM and used as standards to which the optical density of each individual neuron in the same section on that side of the brain or on the opposite side (deprived side) was normalized. A neuron's z-score, therefore, represents the number of standard deviations that its optical density is away from the mean

optical density of the left (intact) NM. This calculation is described by the following formula with OD representing optical density:

$$\text{z-score} = (OD_{\text{individual}} - \text{mean } OD_{\text{left NM}}) / \text{standard deviation of } OD_{\text{left NM}}$$

Z-scores from the same side of all three sections of the same animal were complied as a single database. Frequency histograms of z-scores were graphed for individual animals and complied across all animals in each survival group, referred to as individual and grouped histograms, respectively.

To quantify differences in staining intensity between survival times, the following analyses were conducted. The first analysis examined changes in the overall range of staining intensities between the deprived and control side of the brains at each survival time. The distribution of z-scores in the left NM defines the normal dynamic range of the staining intensity and 95% of neurons have a z-score between 2 and -2. In the right (deprived) NM, z-scores above 2 and below -2 indicate increased and decreased staining intensity, respectively. For the first analysis, the percentages of neurons with z-scores above 2 and below -2, were calculated for the right (deprived) NM of each individual animal. The percentages were used as individual data points for comparisons between different survival groups to unmanipulated animals, using Student's unpaired t-test to determine significance. For the second analysis, z-scores of all neurons in each side of NM in each animal were averaged. The averaged z-scores were used as individual data points for comparison between the deprived and intact sides of the same survival groups using Student's paired t-test. In addition, we compared the average z-scores of the deprived side of each experimental group to unmanipulated animals using Student's unpaired t-test. In the above analyses $p < 0.05$ was considered statistically significant.

Correlation analyses of p-eEF2 immunoreactivity with Y10B immunoreactivity and Nissl stain

These analyses were conducted using fluorescently double-labeled sections. Four animals were used for each correlation analysis. For each animal, 2-3 well-labeled sections were chosen from the

Accepted Article

Accepted Article

intermediate region of NM. For each section, 2-3 images were taken from each side of NM using an Olympus FV-1000 Confocal microscope with a 20x lens. The two fluorescent channels were imaged sequentially to avoid bleed-through between channels. Only neurons with an identifiable cell boundary and a well-defined nucleus were included in the analyses. For each neuron, the integrated optical density of the labeling within the cytoplasm was measured for each channel in the ImageJ software. Once all neurons in an image were measured, the integrated optical density of each neuron was normalized to the median integrated density of all measured NM neurons in the same image and the same channel. The normalized integrated density for p-eEF2 immunoreactivity was graphed in a scatter plot as a function of the normalized integrated density for Y10B immunoreactivity, or as a function of the normalized integrated density for Neurotrace labeling, from neurons within individual sections or by combining all neurons across sections and animals. Pearson's correlation analyses were performed to determine the significance of the correlation between p-eEF2 and Y10B labeling or between p-eEF2 and Neurotrace labeling (Prism, GraphPad Software, La Jolla, California, USA).

Imaging

Digital images of selected sections were captured with a Zeiss Axioplan microscope and collected in SlideBook (Intelligent Imaging Innovations, Inc., Denver, CO) or using confocal microscopy (Fluoview 1000, Olympus, Center Valley, PA). Image brightness and contrast adjustments were performed using Adobe Photoshop (Adobe Systems Inc., Mountain View, CA).

Results

Expression and phosphorylation of eEF2 in normally innervated NM neurons

Accepted Article

The expression and localization of eEF2 in normally innervated NM neurons were examined using an antibody recognizing eEF2 protein independent of its phosphorylation status. Most, if not all, NM neurons exhibit strong eEF2 immunoreactivity in the cytoplasm in contrast to light labeling in the nucleus (Fig. 2A). To validate the use of the left NM as an intra-animal control in evaluating changes in eEF2 immunoreactivity in the right NM following removal of the right cochlea, we quantified relative z-scores of the optical density of eEF2 labeling in individual NM neurons in unmanipulated animals (see Methods). Both the mean and distribution of z-scores are comparable between the left and right NMs in individual animals (Fig. 2E), as well as when neurons from multiple animals are combined (Fig. 2G).

Since eEF2 activity is mostly regulated by its phosphorylation in that eEF2 is inactivated once phosphorylated (Ryazanov et al., 1988), we further examined the level and distribution of p-eEF2 in NM neurons using a phospho-specific (Thr56) eEF2 antibody. As expected, p-eEF2 is mostly concentrated in the cytoplasm of NM neurons (Fig. 2B). Notably, the intensity of p-eEF2 immunoreactivity varies dramatically among individual neurons from virtually background levels to prominent staining, suggesting that individual NM neurons differ from each other in their p-eEF2 level at any given moment under physiological conditions. Although the neurons containing levels of cytoplasmic p-eEF2 labeling as low as the background occur infrequently (2.4 % of all measured neurons in control animals), they often cluster (Fig. 2B, arrowheads) and are found in any part of the NM. We verified that the cells containing little or no p-eEF2 labeling are intact, healthy neurons by double labeling NM neurons with both p-eEF2 and MAP2, a somatodendritic marker. MAP2 labels every neuron in NM (Fig. 2C), while the level of p-eEF2 in the same neurons varies largely (Fig. 2D). Importantly, both the mean and distribution of z-scores of optical density of p-eEF2 are comparable

between the left and right NMs in individual animals (Fig. 2F), as well as when neurons from multiple animals are combined (Fig. 2H).

Unchanged eEF2 protein level following cochlea removal

To explore whether eEF2 protein level is altered in afferent-deprived NM neurons, we examined changes in total eEF2 immunoreactivity between 0.5 to 48 hours following removal of the right cochlea. No notable difference in eEF2 immunoreactivity was detected at any of these times between the left (intact) and the right (deprived) NM neuronal populations (Fig. 3). The distributions of z-scores between the two NMs were largely comparable in individual animals (Fig. 3C, F, I), as well as when neurons from multiple animals were combined, although the dynamic range of z-scores in the deprived NM appeared slightly larger than that in the intact NM at some survival times, in particular at 0.5 hours (Fig. 4). The percentages of deprived neurons having a z-score below -2, between 2 and -2 (representing the 95% confidence interval of the distribution), and above 2, were not significantly different from these values in the intact NM (Fig. 5A; n = 4 to 6 animals for each group; Student's unpaired t-test used for this and all following analyses unless stated otherwise). The mean z-score of eEF2 immunoreactivity of deprived NM neurons was not significantly different from the intact NM in any survival group (Student's paired t-test). In addition, the mean z-score of eEF2 immunoreactivity averaged from all neurons in the deprived NM was not significantly different between the control and each survival group (Fig. 5C). We conclude that afferent deprivation induced by cochlea removal does not significantly alter eEF2 protein levels within 48 hours.

Reduced p-eEF2 level in NM neurons following cochlea removal

Changes in the immunoreactivity for p-eEF2 were then examined at the same time points following cochlea removal. At 0.5 hours following the surgery, more neurons in the deprived NM exhibited p-eEF2 immunoreactivity at very low levels than in the intact NM of the same animal (Fig. 6A-B; n = 6

Accepted Article

Accepted Article

animals). The distribution of z-scores shifted towards negative in individual cases (Fig. 6C), as well as when neurons from all animals in the survival group are combined (Fig. 7A). An average of 23.6% neurons had a z-score less than -2, as compared to 7.6% in the control group, although this difference was not significant (Fig. 5B). The mean z-score of deprived NM neurons was not significantly different from the intact NM at this time point (Student's paired t-test). In addition, the mean z-score averaged from all measured neurons in the deprived NM was smaller than that calculated from the unmanipulated animals, although this difference was not statistically significant (Fig. 5C).

Changes first observed at 0.5 hours became more prominent between 1 and 6 hours. On average, more neurons in the deprived NM exhibited low levels of p-eEF2 immunoreactivity (Fig. 6E, H, K; arrowheads), with 25.6%, 32.4%, and 47.7% neurons having a z-score less than -2 at 1 hour (n = 8 animals), 3 hours (n = 6 animals), and 6 hours (n = 6 animals), respectively, which were all significantly greater percentages than the control (Fig. 5B). The mean z-score of deprived NM neurons was significantly smaller than the intact NM at each of these time points (Student's paired t-test). In addition, the mean z-score averaged from all measured neurons in the deprived NM was significantly smaller than that of unmanipulated animals at these time points (Fig. 5C).

At 12 hours, these changes were seemingly becoming less dramatic: an average of 32.9% neurons had a z-score less than -2 and this was not significantly different from the control (Fig. 5A; n = 6 animals). However, the mean z-score of deprived NM neurons remained significantly smaller than the intact NM at this time point (Student's paired t-test). In addition, the mean z-score averaged from all measured neurons in the deprived NM at 12 hours was significantly smaller than that of unmanipulated animals (Fig. 5C). It is important to note that these less dramatic changes probably resulted from undersampling of neurons with very low levels of p-eEF2 immunoreactivity, instead of indicating a recovery from reduced p-eEF2 immunoreactivity. Some of the neurons may not have

matched the criteria for being included in data analyses due to poorly defined nuclear and cell boundaries at this time. As described below, neurons with low levels of p-eEF2 eventually degrade and die. Interestingly, there were significantly less neurons with a z-score above 2 at 12 hours as compared to the control.

As expected, by 48 hours the volume of the deprived NM was smaller and fewer neurons were visible with p-eEF2 or Nissl staining than the intact NM (data not shown; see Born and Rubel, 1985). The distribution of staining intensities for p-eEF2 immunoreactivity of the surviving deafferented NM neurons was within the normal range of the immunoreactivity in the intact NM (Figs. 5B, 6P-R; and 7F; n = 4 animals) and the mean z-score of deprived NM neurons was not significantly different from the intact NM at this time point (Student's paired t-test). In addition, the mean z-score averaged from all measured neurons in the deprived NM was not significantly different from that of unmanipulated animals (Fig. 5C).

In previous studies we have documented that by about 6 hours following removal of the cochlea, NM neurons segregate into two distinctly different populations, those that will undergo cell death and those that will recover (Steward and Rubel, 1985; Garden et al., 1995; Hartlage-Rübsamen and Rubel, 1996). The distribution pattern of the z-score of p-eEF2 staining in the deprived NM showed individual variation across animals at 0.5 to 12 hours following cochlea removal. In some animals, the z-score distribution of the deprived NM appeared to display two distinct peaks, one at near zero (the control level) and the other more negative (Fig. 6C, F, I, L, O, R; arrows), suggesting that there were two populations of neurons, one with normal levels of p-eEF2 immunoreactivity and the other having reduced p-eEF2 immunoreactivity. In other animals, the distribution of p-eEF2 in the deprived NM exhibited an overall shift from the normal distribution of the intact NM. When z-scores from all animals were combined, no clear bimodality was observed (Fig. 7).

Accepted Article

Accepted Article

In summary, cochlea removal does not lead to significant changes in the intensity of eEF2 immunoreactivity, but does produce significant and rapid reductions in the intensity of p-eEF2 immunoreactivity in NM neurons. Therefore, the observed reductions in p-eEF2 are due to changes in phosphorylation status of existing eEF2 proteins, rather than decreases in the total amount of eEF2 protein.

Correlation of p-eEF2 immunoreactivity to cell survival in NM

To explore the relationship of eEF2 phosphorylation to cell survival and/or death in NM neurons, we examined the correlation between p-eEF2 immunoreactivity and cell death in NM induced by cochlea removal. Dying neurons can be identified by a ghost-like appearance in Nissl-stained sections as early as 12 hours following the surgery, well before their final degradation at 24-48 hours (Born and Rubel, 1985; Steward and Rubel, 1985). We double labeled these NM neurons with p-eEF2 immunocytochemistry and Neurotrace, a fluorescent Nissl marker (Fig. 8). As expected, intensities of both p-eEF2 immunoreactivity and Neurotrace labeling varied greatly across NM neurons, particularly in the deprived NM at 12 hours. Importantly, the level of cytoplasmic Neurotrace labeling was associated with the level of p-eEF2 immunoreactivity; neurons with a lower level of p-eEF2 immunoreactivity tended to have a lower level of Neurotrace labeling (Fig. 8A, B, and D). Correlation analyses revealed significant correlations of normalized intensities of these two types of labeling at the individual cell level in deprived NM (Fig. 8F; n = 460 neurons; $p<0.0001$). In particular, we observed "ghost" neurons with low cytoplasmic and high nuclear Neurotrace labeling (Fig. 8A-B; arrowheads in inserts), indicating a condensed nucleus and the onset of apoptosis. Most, if not all, ghost neurons exhibited no reliable p-eEF2 immunoreactivity above the background level, although not every neuron with low p-eEF2 levels was a ghost neuron (Fig. 8A,B; stars in inserts). Interestingly, we detected a similar and significant correlation of p-eEF2 and Neurotrace labeling in the intact NM of the same

animals (Fig. 8C and 8E; n = 403 neurons; $p<0.0001$), but there is a significant group of cells with low levels of both labels in the deprived group that does not appear on the intact side (box in Fig. 8D).

Correlation of p-eEF2 immunoreactivity to overall protein synthesis in NM

A ghost-like appearance of afferent-deprived NM neurons indicates the onset of apoptosis. To exclude the possibility that the absence of p-eEF2 immunoreactivity in ghost neurons is purely a result of compromised cell integrity, we aimed to explore the correlation of p-eEF2 level with cell survival at an earlier time point before the onset of irreversible apoptosis. To achieve this goal, we double labeled NM neurons with p-eEF2 and Y10B immunocytochemistry at 6 hours following cochlea removal. Y10B is a reliable marker for the overall rate of protein synthesis and cell survival in NM neurons at 6 hours following cochlea removal (Garden et al., 1994). More importantly, deprived NM neurons can be rescued from death by restoring afferent activity at 6 hours, which recovers synthetic and metabolic activities of deprived NM neurons (Born and Rubel, 1988). Similar to what we found by double labeling with p-eEF2 and Neurotrace, intensities of both p-eEF2 and Y10B immunoreactivity varied greatly across neurons in deprived and intact NM (Fig. 9) and the level of cytoplasmic Y10B is highly correlated with the level of p-eEF2 on both sides of the brain (Fig. 9; n's = 460 and 406, respectively; $p's < 0.0001$). Again, examining the raw date from individual cases revealed a significant group of neurons with abnormally low levels of both labels in the deprived NM, which does not appear on the intact side. Representative examples from individual case are shown in Fig. 9C and D.

Discussion

This study examines changes in eEF2 activity following deprivation of excitatory afferent input and explores its involvement in protein synthesis regulation and cell survival in the chicken NM. Our data

Accepted Article

Accepted Article

demonstrate three major conclusions. First, under normally innervated conditions, individual NM neurons differ in p-eEF2 level at any given biological moment. Second, afferent input dramatically regulates eEF2 activity posttranslationally in NM neurons. Afferent deprivation causes rapid decreases in the level of p-eEF2 but not total eEF2. Third, the level of p-eEF2 in individual NM neurons is associated with the overall rate of protein translation and cell survival at later time points following afferent deprivation. Potential mechanisms underlying afferent regulation of eEF2 phosphorylation, as well as functional implications of eEF2 phosphorylation in protein translation and cell survival are discussed below.

Afferent regulation of eEF2 activity

Afferent deprivation leads to posttranslational modification of eEF2 in NM neurons, consistent with the notion that eEF2 activity is mostly regulated by phosphorylation and dephosphorylation (Kaul et al., 2011). Given that eEF2 has a half-life of greater than 16 hours (Terada et al., 1994), it is not surprising that no significant change in the total level of eEF2 is detected in deprived NM neurons within 12 hours despite a dramatic reduction in global protein synthesis during this period (Steward and Rubel, 1985; Born and Rubel, 1988). However, it is worth noting that eEF2 protein level is subject to regulation of intrinsic neuronal activity at the subcellular level. For example, neuronal activity evoked by high potassium regulates total eEF2 in nerve growth cones (Iizuka et al., 2007).

We believe that neurotransmission interruption that is induced by cochlea removal is responsible for the observed reduction in the level of p-eEF2 in NM neurons. Cochlea removal leads to immediate cessation of action potentials of the auditory nerve and NM neurons (Born et al., 1991), death of ganglion cells does not occur for 24 hours or longer, and degenerating axons are not detected in NM until 48 – 72 hours (Lurie and Rubel, 1994). In a number of neuronal types, eEF2 phosphorylation is strongly correlated with sensory stimulation (Scheetz et al., 1997), glutamate

application (Marin et al., 1997; Lenz and Avruch, 2005), and activation of metabotropic or ionotropic glutamate receptors (Marin et al., 1997; Scheetz et al., 1997, 2000; Chotiner et al., 2003; Sutton et al., 2004, 2006, 2007; Cossenza et al., 2006; Nosyreva and Kavalali, 2010; Autry et al., 2011). In addition, blocking action potential-mediated transmission rapidly regulates the level of p-eEF2 in cultured hippocampus neurons (Piccoli et al., 2007; Sutton et al., 2007; Verpelli et al., 2010). Verpelli et al. (2010) further reported that this regulation has differential effects on eEF2 phosphorylation in dendrites and the soma, which is consistent with 5-hydroxytryptamine (5-HT) neurotransmission having opposite effects on eEF2 phosphorylation in neurites and the soma of aplysia sensory neurons (Weatherill et al., 2011). This subcellular specificity suggests that neurotransmission regulation of eEF2 activity is tightly associated with its specific function on site. Chicken NM neurons are mostly adendritic, providing a relatively simple model to explore cellular and molecular events involved in rapid regulation of eEF2 phosphorylation by neurotransmission.

Multiple mechanisms may be involved in the reduction in the level of p-eEF2 in afferent-deprived NM neurons. Such a reduction can result from a combination of a decrease in eEF2 phosphorylation and/or an active increase in eEF2 dephosphorylation. eEF2 phosphorylation is mostly controlled by eEF2 kinase, a calcium/calmodulin dependent kinase (Kaul et al., 2011). Calcium elevation or influx increases eEF2 phosphorylation through activation of eEF2 kinase (Marin et al., 1997; Iizuka et al., 2007; Chen et al., 2009). Since the eEF2 phosphorylation system has a rapid turnover rate (Gschwendt et al., 1988; Arora et al., 2005), the level of p-eEF2 in a cell is largely controlled by the activity of eEF2 kinase. In chick NM, afferent deprivation leads to a rapid increase in the basal level of intracellular calcium concentration (Zirpel et al., 1995 a; b; Zirpel and Rubel, 1996), which presumably should activate eEF2 kinase and thus enhance eEF2 phosphorylation, opposite to what we observed. This paradox implicates additional regulatory pathways in controlling the level of

Accepted Article

p-eEF2 in NM neurons, such as cAMP-dependent protein kinase, which controls eEF2 kinase activity by phosphorylation (Mitsui et al., 1993; Redpath and Proud, 1993), or protein phosphatase 2A, which dephosphorylates eEF2 (Gschwendt et al., 1989). This suggestion is supported by a report that the induction of eEF2 phosphorylation by alcohol is controlled by an increase in cAMP-activated protein kinase, but not eEF2 kinase, and a decrease in protein phosphatase 2A activity (Hong-Brown et al., 2007).

We are unable to determine whether afferent deprivation affects the level of p-eEF2 in all, or only a subpopulation of, deprived NM neurons. It appears that in some animals a substantial percentage of deprived NM neurons maintain normal levels of p-eEF2, suggesting that they either start with a high level of p-eEF2 before the manipulations or undergo no or relatively small reductions following the manipulations. Dynamic approaches that are able to monitor the same neurons before and after afferent deprivation will help clarify this issue.

eEF2 phosphorylation and protein synthesis

It has been well documented that phosphorylation inactivates eEF2, leading to decreased protein synthesis (Ryazanov et al., 1988; Carlberg et al., 1990; Redpath et al., 1993). In non-neuronal cell types, phosphorylation of eEF2 correlates with decreased translation during mitosis (Celis et al., 1990) and energy deprivation (Horman et al., 2002). Consistently, insulin-stimulated eEF2 dephosphorylation leads to enhanced protein synthesis (Redpath et al., 1996; Diggle et al., 1998; Wang et al., 2000). In addition, in hippocampal neurons activity-dependent phosphorylation of eEF2 inhibits local protein translation in dendrites while dephosphorylation promotes local translation (Sutton et al., 2007).

In the chicken NM, cochlea removal causes a dramatic reduction in protein synthesis in all deprived NM neurons at 0.5-3 hours (Steward and Rubel, 1985; Born and Rubel, 1988). If this reduction results from changes in eEF2 phosphorylation, we would expect to see *increases* in eEF2

Accepted Article

Accepted Article

phosphorylation in *all* deprived NM neurons. Unexpectedly, we observed dramatic *decreases* in eEF2 phosphorylation in a large number of deprived NM neurons. This paradox raises the possibility that afferent regulated eEF2 phosphorylation does not account for the initial reductions in protein synthesis.

Protein synthesis regulators other than eEF2 may be responsible for the initial decrease in translation. Candidates include other elongation factors such as eEF1 (Scheetz et al., 2000; Browne and Proud, 2002), whose translation and phosphorylation are also regulated by glutamate and neuronal activity (Antion et al., 2008; Grange et al., 2009; Barrera et al., 2010). In addition, regulation of protein synthesis may take place at the initiation step of protein translation (Nakamoto, 2009; Sonenberg and Hinnebusch, 2009; Hernández et al., 2010; Jackson et al., 2010). It is interesting to note that regulation of the initiation and elongation steps can take place simultaneously but selectively alter different subcellular compartments (Kanhema et al., 2006).

Although eEF2 dephosphorylation is unlikely to be responsible for the initial broad decrease in protein synthesis, the current study demonstrates that the overall rate of protein synthesis is correlated with the level of p-eEF2. At later time points following cochlear removal (6 and 12 hours), neurons that are apparently unable to regain synthetic activity are the ones with abnormally lower levels of p-eEF2. This observation suggests that eEF2 phosphorylation is associated with signaling critical for the recovery of protein synthesis. Identification of the inducer(s) of protein suppression in NM neurons is required to further elaborate the relationship between protein synthesis and eEF2 phosphorylation.

It is interesting to know how eEF2 phosphorylation is related to protein synthesis in the intact NM. The current study demonstrates that p-eEF2 level is highly correlated with Y10B intensity in intact NM; neurons with a higher level of p-eEF2 tend to have a higher level of Y10B. If we assume that the level of Y10B is similarly correlated with the rate of protein synthesis in intact NM as in deprived NM, this observation would suggest that neurons with a low level of p-eEF2 probably have a

Accepted Article

low rate of protein synthesis. Hence, the overall protein synthesis in intact NM neurons may not be regulated by phosphorylation of eEF2 in a similar way as in other systems. Alternatively, it is possible that the amount of active (unphosphorylated) eEF2 in both normally innervated and deprived NM neurons is sufficient for protein synthesis, while the level of p-eEF2 is associated with protein synthesis and other cellular events through distinct mechanisms. If a certain condition causes an increase in phosphorylation of eEF2 to a level that there is no enough active eEF2 for overall protein synthesis, a correlation of p-eEF2 with protein synthesis may be observed in the expected manner, i.e., neurons with a lower level of p-eEF2 tend to have a higher level of protein synthesis.

eEF2 phosphorylation and cell survival/death

eEF2 phosphorylation-mediated cell survival and apoptosis has been documented in a number of systems. It appears that this mediation acts through two distinct mechanisms. The first mechanism is through eEF2 phosphorylation-induced suppression of *overall* protein translation. It is proposed that suppression of protein synthesis first affects anti-apoptotic proteins since they are disproportionately short lived relative to their pro-apoptotic counterparts (reviewed in White-Gilbertson et al., 2008). This proposal is supported by the requirement of the presence and activity of anti-apoptotic proteins and active translational machinery for cell survival (Adams and Cooper, 2007; Willis et al., 2007). eEF2 phosphorylation and the resulting suppression of protein translation may also have protective effects against excitotoxicity-induced neuronal death, although the exact processes remain unknown (Marin et al., 1997). The second mechanism of eEF2 phosphorylation-mediated cell survival is associated with the function of p-eEF2 in promoting a number of *specific* proteins. For example, eEF2 phosphorylation-mediated Bcl-xL synthesis is critical for the growth and survival of cancer cells (Arora et al., 2003; Wu et al., 2006; Nakamura et al., 2009; Zhang et al., 2011).

Accepted Article

The data presented here and several previous studies suggest a novel pattern of eEF2 phosphorylation-mediated cell survival and death. Following afferent deprivation, NM neurons with relatively high levels of p-eEF2 tend to have a healthier looking in Nissl staining and ribosomal RNA (reported byY10B immunoreactivity), and presumably tend to survive. Consistently, dying neurons always exhibit a low level of p-eEF2. Deprivation induced cell death probably result from persistent protein synthesis suppression affecting the levels of apoptotic and anti-apoptotic proteins differentially. Cell survival following the same manipulation is likely due to the recovery of protein synthesis and/or other survival signals initiated or upregulated by p-eEF2. Among identified proteins whose synthesis is promoted by eEF2 phosphorylation, brain-derived neurotrophic factor (Verpelli et al., 2010; Autry et al., 2011), Arc/Arg3.1 (Park et al., 2008; Kuipers et al., 2009), and Bcl-xL (Zhang et al., 2011) have been associated with cell survival and apoptosis. Whether these proteins are involved in eEF2 phosphorylation-mediated cell protection and apoptosis following afferent deprivation requires further investigation. It is interesting to point out that Bcl-2, another Bcl-2 family member like Bcl-xL, is expressed in NM and AVCN neurons. Overexpression or pharmacologically induced increases in the level of Bcl-2 have been shown to prevent afferent deprivation-induced cell death in NM and AVCN neurons (Mostafapour et al., 2002; Bush and Hyson, 2006). However, it is less clear whether Bcl-2 is involved in determining cell fate in this type of cell death, since the time course of changes in Bcl-2 protein level following cochlea removal has not been determined, although Bcl-2 mRNA level is altered at long term survival times (Wilkinson et al., 2002; Harris et al., 2008).

Finally, it must be pointed out that loss of p-eEF2 may not necessarily indicate ensuing cell death. A number of deprived NM neurons exhibit no or little p-eEF2 but do not have a “ghost”-like appearance at 12 hours following cochlea removal. One possibility is that a threshold level of p-eEF2 is required for cell survival and these neurons lacking p-eEF2 may turn into “ghost cells” later and

subsequently die. Alternatively, these neurons may survive, a possibility that would suggest the involvement of survival signaling initiated by cellular events beyond the p-eEF2 mechanism.

Other Acknowledgments

We thank Glen MacDonald for help with imaging and data quantification, Claire Walker and Mark Hudson for Western blotting, and Joan Steitz for originally providing the Y10B antibody.

Conflict of Interest Statement

There is no identified conflict.

Role of Authors

All authors had full access to all the data in the study and take responsibility for the integrity of the data and the accuracy of the data analysis. Study concept and design: EWR and YW. Acquisition of data: EGM and YW. Analysis and interpretation of data: EGM and YW. Drafting of the manuscript: EGM and YW. Critical revision of the manuscript for important intellectual content: YW and EWR. Statistical analysis: EGM. Obtained funding: EWR.

References

Adams KW, Cooper GM. 2007. Rapid Turnover of MCL-1 Couples Translation To Cell Survival and Apoptosis. J Biol Chem 282:6192–6200.

Antion MD, Hou L, Wong H, Hoeffer CA, Klann E. 2008. mGluR-Dependent Long-Term Depression Is Associated with Increased Phosphorylation of S6 and Synthesis of Elongation Factor 1A but Remains Expressed in S6K-Deficient Mice. Mol Cell Biol 28:2996–3007.

Accepted Article

Arora S, Yang J-M, Hait WN. 2005. Identification of the Ubiquitin-Proteasome Pathway in the Regulation of the Stability of Eukaryotic Elongation Factor-2 Kinase. Cancer Res 65:3806–3810.

Arora S, Yang J-M, Kinzy TG, Utsumi R, Okamoto T, Kitayama T, Ortiz PA, Hait WN. 2003. Identification and Characterization of an Inhibitor of Eukaryotic Elongation Factor 2 Kinase against Human Cancer Cell Lines. Cancer Res 63:6894 –6899.

Autry AE, Adachi M, Nosyreva E, Na ES, Los MF, Cheng P, Kavalali ET, Monteggia LM. 2011. NMDA Receptor Blockade at Rest Triggers Rapid Behavioural Antidepressant Responses. Nature 475:91–95.

Bagaglio DM, Cheng EHC, Gorelick FS, Mitsui K-I, Nairn AC, Hait WN. 1993. Phosphorylation of Elongation Factor 2 in Normal and Malignant Rat Glial Cells. Cancer Res 53:2260–2264.

Barrera I, Flores-Méndez M, Hernández-Kelly LC, Cid L, Huerta M, Zinker S, López-Bayghen E, Aguilera J, Ortega A. 2010. Glutamate regulates eEF1A phosphorylation and ribosomal transit time in Bergmann glial cells. Neurochem Int 57:795–803.

Born DE, Durham D, Rubel EW. 1991. Afferent influences on brainstem auditory nuclei of the chick: Nucleus magnocellularis neuronal activity following cochlea removal. Brain Res 557:37–47.

Born DE, Rubel EW. 1985. Afferent influences on brain stem auditory nuclei of the chicken: neuron number and size following cochlea removal. J Comp Neurol 231:435–445.

Born DE, Rubel EW. 1988. Afferent influences on brain stem auditory nuclei of the chicken: presynaptic action potentials regulate protein synthesis in nucleus magnocellularis neurons. J Neurosci 8:901–919.

Browne GJ, Proud CG. 2002. Regulation of peptide□chain elongation in mammalian cells. Eur J Biochem 269:5360–5368.

Accepted Article

Accepted Article

Bush AL, Hyson RL. 2006. Lithium increases bcl-2 expression in chick cochlear nucleus and protects against deafferentation-induced cell death. Neuroscience 138:1341–1349.

Carlberg U, Nilsson A, Nygård O. 1990. Functional properties of phosphorylated elongation factor 2. Eur J Biochem 191:639–645.

Celis JE, Madsen P, Ryazanov AG. 1990. Increased phosphorylation of elongation factor 2 during mitosis in transformed human amnion cells correlates with a decreased rate of protein synthesis. Proc Natl Acad Sci U S A 87:4231–4235.

Chen JH, Riazy M, Smith EM, Proud CG, Steinbrecher UP, Duronio V. 2009. Oxidized LDL-Mediated Macrophage Survival Involves Elongation Factor-2 Kinase. Arterioscler Thromb Vasc 29:92–98.

Chen Z, Gopalakrishnan SM, Bui M-H, Soni NB, Warrior U, Johnson EF, Donnelly JB, Glaser KB. 2011. 1-Benzyl-3-cetyl-2-methylimidazolium iodide (NH125) Induces Phosphorylation of Eukaryotic Elongation Factor-2 (eEF2). J Biol Chem 286:43951 –43958.

Cheng EH, Gorelick FS, Czernik AJ, Bagaglio DM, Hait WN. 1995. Calmodulin-dependent protein kinases in rat glioblastoma. Cell Growth Differ 6:615.

Chotiner J., Khorasani H, Nairn A., O'Dell T., Watson J. 2003. Adenylyl cyclase-dependent form of chemical long-term potentiation triggers translational regulation at the elongation step. Neuroscience 116:743–752.

Clarke PG, Egloff M. 1988. Combined effects of deafferentation and de-efferentation on isthmo-optic neurons during the period of their naturally occurring cell death. Anat Embryol 179:103–108.

Cossenza M, Cadilhe DV, Coutinho RN, Paes□de□Carvalho R, Cossenza M, Cadilhe DV, Coutinho RN, Paes□de□Carvalho R. 2006. Inhibition of protein synthesis by activation of NMDA

receptors in cultured retinal cells: a new mechanism for the regulation of nitric oxide production. J Neurochem 97:1481–1493.

Diggle TA, Redpath NT, Heesom KJ, Denton RM. 1998. Regulation of protein-synthesis elongation-factor-2 kinase by cAMP in adipocytes. Biochem J 336:525–529.

Garden G, Canady K, Lurie D, Bothwell M, Rubel E. 1994. A biphasic change in ribosomal conformation during transneuronal degeneration is altered by inhibition of mitochondrial, but not cytoplasmic protein synthesis. J Neurosci 14:1994–2008.

Garden GA, Hartlage-Rübsamen M, Rubel EW, Bothwell MA. 1995a. Protein Masking of a Ribosomal RNA Epitope Is an Early Event in Afferent Deprivation-Induced Neuronal Death. Mol Cell Neurosci 6:293–310.

Garden GA, Redeker-DeWulf V, Rubel EW. 1995b. Afferent influences on brainstem auditory nuclei of the chicken: regulation of transcriptional activity following cochlea removal. J Comp Neurol 359:412–423.

Grange J, Belly A, Dupas S, Trembleau A, Sadoul R, Goldberg Y. 2009. Specific interaction between Sam68 and neuronal mRNAs: implication for the activity-dependent biosynthesis of elongation factor eEF1A. J Neurosci Res 87:12–25.

Gschwendt M, Kittstein W, Marks F. 1988. Ciclosporin inhibits phorbol-ester-induced hyperplastic transformation and tumor promotion in mouse skin probably by suppression of Ca2+/calmodulin-dependent processes such as phosphorylation of elongation factor 2. Skin Pharmacol. 1:84–92.

Gschwendt M, Kittstein W, Mieskes G, Marks F. 1989. A type 2A protein phosphatase dephosphorylates the elongation factor 2 and is stimulated by the phorbol ester TPA in mouse epidermis in vivo. FEBS Letters 257:357–360.

Accepted Article

Guillery RW. 1973. Quantitative studies of transneuronal atrophy in the dorsal lateral geniculate nucleus of cats and kittens. J Comp Neurol 149:423–437.

Harris JA, Iguchi F, Seidl AH, Lurie DI, Rubel EW. 2008. Afferent deprivation elicits a transcriptional response associated with neuronal survival after a critical period in the mouse cochlear nucleus. J Neurosci 28:10990–11002.

Hartlage-Rübsamen M, Rubel EW. 1996. Influence of mitochondrial protein synthesis inhibition on deafferentation-induced ultrastructural changes in nucleus magnocellularis of developing chicks. J Comp Neurol 371:448-460.

Hashisaki GT, Rubel EW. 1989. Effects of unilateral cochlea removal on anteroventral cochlear nucleus neurons in developing gerbils. J Comp Neurol 283:5–73.

Heil P, Scheich H. 1986. Effects of unilateral and bilateral cochlea removal on 2-deoxyglucose patterns in the chick auditory system. J Comp Neurol 252:279–301.

Hernández G, Altmann M, Lasko P. 2010. Origins and evolution of the mechanisms regulating translation initiation in eukaryotes. Trends Biochem Sci 35:63–73.

Hong-Brown LQ, Brown CR, Huber DS, Lang CH. 2007. Alcohol Regulates Eukaryotic Elongation Factor 2 Phosphorylation Via an AMP-Activated Protein Kinase-Dependent Mechanism in C2C12 Skeletal Myocytes. J Biol Chem 282:3702–3712.

Horman S, Browne GJ, Krause U, Patel JV, Vertommen D, Bertrand L, Lavoinne A, Hue L, Proud CG, Rider MH. 2002. Activation of AMP-Activated Protein Kinase Leads to the Phosphorylation of Elongation Factor 2 and an Inhibition of Protein Synthesis. Current Biology 12:1419–1423.

Hyson RL, Rubel EW. 1995. Activity-dependent regulation of a ribosomal RNA epitope in the chick cochlear nucleus. Brain Res 672:196–204.

Accepted Article

Iizuka A, Sengoku K, Iketani M, Nakamura F, Sato Y, Matsushita M, Nairn AC, Takamatsu K, Goshima Y, Takei K. 2007. Calcium-induced synergistic inhibition of a translational factor eEF2 in nerve growth cones. Biochem Bioph Res Co 353:244–250.

Jackson RJ, Hellen CUT, Pestova TV. 2010. The mechanism of eukaryotic translation initiation and principles of its regulation. Nat Rev Mol Cell Bio 11:113–127.

Jørgensen R, Merrill AR, Andersen GR. 2006. The life and death of translation elongation factor 2. Biochem Soc Trans 34:1–6.

Kalil R. 1980. A quantitative study of the effects of monocular enucleation and deprivation on cell growth in the dorsal lateral geniculate nucleus of the cat. J Comp Neurol 189:483–524.

Kanhema T, Dagestad G, Panja D, Tiron A, Messaoudi E, Håvik B, Ying S, Nairn AC, Sonenberg N, Bramham CR, et al. 2006. Dual regulation of translation initiation and peptide chain elongation during BDNF□induced LTP in vivo: evidence for compartment□specific translation control. J Neurochem 99:1328–1337.

Karnes HE, Kaiser CL, Durham D. 2009. Deafferentation-induced caspase-3 activation and DNA fragmentation in chick cochlear nucleus neurons. Neuroscience 159:804–818.

Karnes HE, Scaletty PN, Durham D. 2010. Histochemical and Fluorescent Analyses of Mitochondrial Integrity in Chick Auditory Neurons following Deafferentation. J Am Acad Audiol 21:204–218.

Kaul G, Pattan G, Rafeequi T. 2011. Eukaryotic elongation factor-2 (eEF2): its regulation and peptide chain elongation. Cell Biochem Funct 29:227–234.

Kim HK, Kim Y-B, Kim E-G, Schuman E. 2005. Measurement of dendritic mRNA transport using ribosomal markers. Biochem Biophys Res Commun 328:895–900.

Accepted Article

Kuipers SD, Tiron A, Soule J, Messaoudi E, Trentani A, Bramham CR. 2009. Selective Survival and Maturation of Adult-Born Dentate Granule Cells Expressing the Immediate Early Gene Arc/Arg3.1. PLoS ONE 4:1–12.

Lenz G, Avruch J. 2005. Glutamatergic Regulation of the p70S6 Kinase in Primary Mouse Neurons. J Biol Chem 280:38121–38124.

Lerner EA, Lerner MR, Janeway CA, Steitz JA. 1981. Monoclonal antibodies to nucleic acid-containing cellular constituents: probes for molecular biology and autoimmune disease. Proc Natl Acad Sci U S A 78:2737–2741.

Lurie DI, Rubel EW. 1994. Astrocyte proliferation in the chick auditory brainstem following cochlea removal. J. Comp. Neurol. 346:276–288.

Marin P, Nastiuk KL, Daniel N, Girault J-A, Czernik AJ, Glowinski J, Nairn AC, Prémont J. 1997. Glutamate-Dependent Phosphorylation of Elongation Factor-2 and Inhibition of Protein Synthesis in Neurons. J Neurosci 17:3445 –3454.

Mitsui K, Brady M, Palfrey HC, Nairn AC. 1993. Purification and Characterization of Calmodulin-Dependent Protein Kinase III from Rabbit Reticulocytes and Rat Pancreas. J Biol Chem 268:13422–13433.

Moore DR. 1990. Auditory brainstem of the ferret: early cessation of developmental sensitivity of neurons in the cochlear nucleus to removal of the cochlea. J Comp Neurol 302:810–823.

Mostafapour SP, Cochran SL, Del Puerto NM, Rubel EW. 2000. Patterns of cell death in mouse anteroventral cochlear nucleus neurons after unilateral cochlea removal. J Comp Neurol 426:561–571.

Accepted Article

Mostafapour SP, Del Puerto NM, Rubel EW. 2002. Bcl-2 Overexpression Eliminates Deprivation-Induced Cell Death of Brainstem Auditory Neurons. J Neurosci 22:4670–4674.

Nairn AC, Palfrey HC. 1987. Identification of the major Mr 100,000 substrate for calmodulin-dependent protein kinase III in mammalian cells as elongation factor-2. J Biol Chem 262:17299–17303.

Nakamoto T. 2009. Evolution and the universality of the mechanism of initiation of protein synthesis. Gene 432:1–6.

Nakamura J, Aoyagi S, Nanchi I, Nakatsuka S-I, Hirata E, Shibata S, Fukuda M, Yamamoto Y, Fukuda I, Tatsumi N, et al. 2009. Overexpression of eukaryotic elongation factor eEF2 in gastrointestinal cancers and its involvement in G2/M progression in the cell cycle. Int J Oncol 34:1181–1189.

Nosyreva E, Kavalali ET. 2010. Activity-dependent augmentation of spontaneous neurotransmission during endoplasmic reticulum stress. J Neurosci 30:7358–7368.

Park S, Park JM, Kim S, Kim J-A, Shepherd JD, Smith-Hicks CL, Chowdhury S, Kaufmann W, Kuhl D, Ryazanov AG, et al. 2008. Elongation Factor 2 and Fragile X Mental Retardation Protein Control the Dynamic Translation of Arc/Arg3.1 Essential for mGluR-LTD. Neuron 59:70–83.

Parmer TG, Ward MD, Yurkow EJ, Vyas VH, Kearney TJ, Hait WN. 1999. Activity and regulation by growth factors of calmodulin-dependent protein kinase III (elongation factor 2-kinase) in human breast cancer. Br J Cancer 79:59–64.

Piccoli G, Verpelli C, Tonna N, Romorini S, Alessio M, Nairn AC, Bachi A, Sala C. 2007. Proteomic Analysis of Activity-Dependent Synaptic Plasticity in Hippocampal Neurons. J Proteome Res 6:3203–3215.

Accepted Article

Redpath NT, Foulstone EJ, Proud CG. 1996. Regulation of translation elongation factor-2 by insulin via a rapamycin-sensitive signalling pathway. EMBO J 15:2291–2297.

Redpath NT, Price NT, Severinov KV, Proud CG. 1993. Regulation of elongation factor-2 by multisite phosphorylation. Eur J Biochem 213:689–699.

Redpath NT, Proud CG. 1993. Cyclic AMP-dependent protein kinase phosphorylates rabbit reticulocyte elongation factor-2 kinase and induces calcium-independent activity. Biochem J 293:31–34.

Robinson AM, Conley D, Kern R. 2003. Olfactory neurons in bax knockout mice are protected from bulbectomy-induced apoptosis. NeuroReport 14:1891–1894.

Rubel EW, Fritzsch B. 2002. Auditory System Development: Primary Auditory Neurons and Their Targets. Annu Rev Neurosci 25:51–101.

Ryazanov AG, Shestakova EA, Natapov PG. 1988. Phosphorylation of elongation factor 2 by EF-2 kinase affects rate of translation. Nature 334:170–173.

Scheetz AJ, Nairn AC, Constantine-Paton M. 1997. N-methyl-d-aspartate receptor activation and visual activity induce elongation factor-2 phosphorylation in amphibian tecta: A role for N-methyl-d-aspartate receptors in controlling protein□synthesis. Proc Natl Acad Sci USA 94:14770 –14775.

Scheetz AJ, Nairn AC, Constantine-Paton M. 2000. NMDA receptor-mediated control of protein synthesis at developing synapses. Nat Neurosci 3:211–216.

Sonenberg N, Hinnebusch AG. 2009. Regulation of Translation Initiation in Eukaryotes: Mechanisms and Biological Targets. Cell 136:731–745.

Accepted Article

Steward O, Rubel EW. 1985. Afferent influences on brain stem auditory nuclei of the chicken: cessation of amino acid incorporation as an antecedent to age-dependent transneuronal degeneration. J Comp Neurol 231:385–395.

Sutton MA, Ito HT, Cressy P, Kempf C, Woo JC, Schuman EM. 2006. Miniature Neurotransmission Stabilizes Synaptic Function via Tonic Suppression of Local Dendritic Protein Synthesis. Cell 125:785–799.

Sutton MA, Taylor AM, Ito HT, Pham A, Schuman EM. 2007. Postsynaptic Decoding of Neural Activity: eEF2 as a Biochemical Sensor Coupling Miniature Synaptic Transmission to Local Protein Synthesis. Neuron 55:648–661.

Sutton MA, Wall NR, Aakalu GN, Schuman EM. 2004. Regulation of dendritic protein synthesis by miniature synaptic events. Science 304:1979–1983.

Terada N, Patel HR, Takase K, Kohno K, Nairn AC, Gelfand EW. 1994. Rapamycin selectively inhibits translation of mRNAs encoding elongation factors and ribosomal proteins. Proc Natl Acad Sci USA 91:11477.

Tierney TS, Russell FA, Moore DR. 1997. Susceptibility of developing cochlear nucleus neurons to deafferentation□induced death abruptly ends just before the onset of hearing. J Comp Neurol 378:295–306.

Trune DR. 1982. Influence of neonatal cochlear removal on the development of mouse cochlear nucleus: I. Number, size, and density of its neurons. J Comp Neurol 209:409–424.

Vankirk AM, Byrd CA. 2003. Apoptosis following peripheral sensory deafferentation in the olfactory bulb of adult zebrafish. J Comp Neurol 455:488–498.

Accepted Article

Verpelli C, Piccoli G, Zibetti C, Zanchi A, Gardoni F, Huang K, Brambilla D, Di Luca M, Battaglioli E, Sala C. 2010. Synaptic activity controls dendritic spine morphology by modulating eEF2-dependent BDNF synthesis. J Neurosci 30:5830–5842.

Wang L, Wang X, Proud CG. 2000. Activation of mRNA translation in rat cardiac myocytes by insulin involves multiple rapamycin-sensitive steps. Am J Physiol Heart Circ Physiol 278:H1056–H1068.

Wang Y, Cunningham DE, Tempel BL, Rubel EW. 2009. Compartment-Specific Regulation of Plasma Membrane Calcium ATPase Type 2 in the Chick Auditory Brainstem. J Comp Neurol 514:624–640.

Wang Y, Rubel EW. 2008. Rapid regulation of microtubule-associated protein 2 in dendrites of nucleus laminaris of the chick following deprivation of afferent activity. Neuroscience 154:381–389.

Weatherill DB, McCamphill PK, Pethoukov E, Dunn TW, Fan X, Sossin WS. 2011. Compartment□ specific, differential regulation of eukaryotic elongation factor 2 and its kinase within Aplysia sensory neurons. J Neurochem 117:841–855.

White-Gilbertson S, Rubinchik S, Voelkel-Johnson C. 2008. Transformation, translation and TRAIL: an unexpected intersection. Cytokine Growth F R 19:167–172.

Wilkinson B., Elam J., Fadool D., Hyson R. 2003. Afferent regulation of cytochrome-c and active caspase-9 in the avian cochlear nucleus. Neuroscience 120:1071–1079.

Wilkinson BL, Sadler KA, Hyson RL. 2002. Rapid deafferentation-induced upregulation of bcl-2 mRNA in the chick cochlear nucleus. Mol Brain Res 99:67–74.

Accepted Article

Willis SN, Fletcher JI, Kaufmann T, Van Delft MF, Chen L, Czabotar PE, Ierino H, Lee EF, Fairlie WD, Bouillet P, et al. 2007. Apoptosis Initiated When BH3 Ligands Engage Multiple Bcl-2 Homologs, Not Bax or Bak. Science 315:856–859.

Wu H, Yang J-M, Jin S, Zhang H, Hait WN. 2006. Elongation Factor-2 Kinase Regulates Autophagy in Human Glioblastoma Cells. Cancer Res 66:3015 –3023.

Yamaguchi S, Fujii-Taira I, Murakami A, Hirose N, Aoki N, Izawa E-I, Fujimoto Y, Takano T, Matsushima T, Homma KJ. 2008. Up-regulation of microtubule-associated protein 2 accompanying the filial imprinting of domestic chicks (Gallus gallus domesticus). Brain Res Bull 76:282–288.

Yamaguchi S, Katagiri S, Aoki N, Iikubo E, Kitajima T, Matsushima T, Homma KJ. 2011. Molecular function of microtubule-associated protein 2 for filial imprinting in domestic chicks (Gallus gallus domesticus). Neurosci Res 69:32–40.

Zhang Y, Cheng Y, Zhang L, Ren X, Huber-Keener KJ, Lee S, Yun J, Wang HG, Yang JM. 2011. Inhibition of eEF-2 kinase sensitizes human glioma cells to TRAIL and down-regulates Bcl-xL expression. Biochem Bioph Res Co 414:129–134.

Zirpel L, Lachica EA, Lippe WR. 1995a. Deafferentation Increases the Intracellular Calcium of Cochlear Nucleus Neurons in the Embryonic Chick. J Neurophysiol 74:1355–1357.

Zirpel L, Lachica EA, Rubel EW. 1995b. Activation of a Metabotropic Glutamate Receptor Increases Intracellular Calcium Concentrations in Neurons of the Avian Cochlear Nucleus. J Neurosci 15:214–222.

Accepted Article

Zirpel L, Rubel EW. 1996. Eighth Nerve Activity Regulates Intracellular Calcium Concentration of Avian Cochlear Nucleus Neurons Via a Metabotropic Glutamate Receptor. J Neurophysiol 76:4127–4139.

Accepted Article

Accepted Article

Figure legends

Figure 1: Western blot assay of anti-eEF2 and anti-p-eEF2 in HEK293 cells (**A**) and in chick dorsocaudal brainstem (**B**). Molecular weight standards (left) were used to determine relative sizes of labeled proteins. Anti-eEF2 detects a single band of approximately 95 kDa in both HEK293 cells and chick brainstem regardless of phosphatase treatment. Anti-p-eEF2 detects a single band of the same molecular weight in chick brainstem and HEK293 cells under normal conditions, but is absent in HEK293 cells following phosphatase treatment.

Figure 2: Immunoreactivity for eEF2 and p-eEF2 in normally innervated NM neurons. **A-B:** Differential interference contrast (DIC) images of NM neurons labeled by eEF2 (A) or p-eEF2 (B) immunoreactivity. Note high variability of p-eEF2 immunoreactivity across NM neurons. Arrowheads indicate a cluster of very lightly labeled neurons. Image contrast, brightness, and gamma were adjusted for optimum viewing in this and subsequent figures in Adobe Photoshop CS4. Paired sections always had identical manipulations of these properties. **C-D:** Fluorescent images of the same section through NM neurons double labeled for MAP2 (C) and p-eEF2 (D) immunoreactivity. Arrows indicate neurons that exhibit high levels of both MAP2 and p-eEF2, while arrowheads indicate neurons that exhibit a high level of MAP2 and a low level of p-eEF2 labeling. Dashed lines outline the border of two lightly labeled cells in D. **E-F:** Frequency histograms of z-scores of NM neurons labeled for eEF2 (E) or p-eEF2 (F) from an individual animal. **G-H:** Grouped frequency histograms of z-scores of NM neurons labeled for eEF2 (G) or p-eEF2 (H) complied from all control animals. Each neuron represents an individual data point in these histograms. For both eEF2 and p-eEF2 immunoreactivities, the distribution of z-scores is comparable between the left (grey bars) and right (black bars) NMs. Each bar represents the total number or percentage of neurons with a z-score within ±0.5 of the assigned

value of the bin, and this applies to all histograms in this and subsequent figures. Scale bar is 20 μm in A (applies for A-B) and 10 μm in C (applies for C-D).

Figure 3: Time course of eEF2 immunoreactivity at 1h (**A-C**), 6h (**D-F**), and 48h (**G-I**) following unilateral cochlea removal. Each row represents an individual animal from a survival group and is organized from left to right in the following order: an image of the left (intact) NM (for example in the first row, A), an image of the right (deprived) NM (B), and individual frequency histograms of z-scores in both NMs (C). Each neuron represents an individual data point in these histograms. No notable difference in eEF2 immunoreactivity between the intact and deprived NMs is detected at any time points. The distribution of z-scores is comparable between the two NMs at all time points. Scale bar is 20 μm.

Figure 4: Grouped frequency histograms of z-scores of eEF2 immunoreactivity following unilateral cochlea removal at 0.5h (**A**), 1h (**B**), 3h (**C**), 6h (**D**), 12h (**E**), and 48h (**F**). Each neuron represents an individual data point in these histograms. Neurons from all animals within an individual survival group are complied separately for the intact (grey bars) and deprived (black bars) sides. Consistent with individual histograms illustrated in Figure 3, the distribution of z-scores is comparable between the two NMs at all time points.

Accepted Article

Accepted Article

Figure 5: Analyses of changes in eEF2 and p-eEF2 immunoreactivity at the population level. Each animal represents an individual data point in these analyses; means and SEMs are presented. **A-B:** Percent of neurons in deprived NM with z-scores below -2 (left), between -2 and 2 (middle), and above 2 (right) for eEF2 (A) and p-eEF2 (B) immunoreactivities for each survival group. An asterisk above an individual group indicates that the percentage of neurons within each z-score range at that survival time is significantly different ($p < 0.05$) from the control group. **C:** Average z-score of eEF2 (grey bars) and p-eEF2 (black bars) immunoreactivity in deprived NM neurons. An asterisk above individual groups indicates that the z-score of a survival group is significantly different ($p < 0.05$) from the control group.

Figure 6: Time course of p-eEF2 immunoreactivity at 0.5h (**A-C**), 1h (**D-F**), 3h (**G-I**), 6h (**J-L**), 12h (**M-O**), and 48h (**P-R**) following unilateral cochlea removal. Each row represents an individual animal from a survival group and is organized from left to right in the following order: an image of the left (intact) NM (for example in the first row, A), an image of the right (deprived) NM (B), and individual frequency histograms of z-scores in both NMs (C). Each neuron represents an individual data point in these histograms. Arrows and arrowheads in the images indicate examples of darkly and lightly labeled neurons, respectively. Arrows in the histograms point out two visually detectable peaks of the z-score distribution in the deprived NM (black bars). Note not all animals exhibit two readily detected peaks. At 48h, the distribution of the immunoreactivity is comparable between two NMs. Scale bar is 20 μm.

Accepted Article

Figure 7: Grouped frequency histograms of z-scores of p-eEF2 immunoreactivity following unilateral cochlea removal at 0.5h (**A**), 1h (**B**), 3h (**C**), 6h (**D**), 12h (**E**), and 48h (**F**). Each neuron represents an individual data point in these histograms. Neurons from all animals within an individual survival group are complied separately for the intact (grey bars) and deprived (black bars) sides. Consistent with individual histograms illustrated in Figure 6, reductions in p-eEF2 immunoreactivity start at 0.5h, become more prominent between 1-6h, and disappear at 48h.

Figure 8: Correlation of p-eEF2 immunoreactivity with Neurotrace staining in NM neurons at 12h following cochlea removal. **A-B:** Images of p-eEF2 immunoreactivity (A) and Neurotrace labeling (B) in the same section in the deprived NM at 12h following cochlea removal. Neurons with a lower intensity of p-eEF2 labeling tend to have a lower level of Neurotrace labeling. Arrowheads indicate "ghost neurons" without reliable immunoreactivity for p-eEF2. Arrows indicate neurons with high intensities of both labels. Occasionally, neurons with a low level of p-eEF2 have a high level of Neurotrace staining (stars). Dashed lines outline the border of two lightly labeled neurons. White frames indicate the location of the insert. **C-D:** Scatter plots from a representative individual animal with unilateral cochlea removal showing integrative p-eEF2 intensity as a function of integrative Neurotrace intensity in intact (C) and afferent-deprived (D) NM neurons from the same section. Note a group of neurons (Box in D) with abnormally low intensities for both labels present in the deprived, but not the intact, NM. **E-F:** Scatter plots of normalized grouped data; p-eEF2 intensity as a function of normalized Neurotrace intensity in intact (E) or afferent-deprived (F) NM neurons. All cells were combined from multiple sections and animals. Pearson's correlation coefficient and significance are indicated for each plot. Scale bar is 25 μm in A-B and 12.5 μm in inserts.

Accepted Article

Figure 9: Correlation of p-eEF2 immunoreactivity with Y10B immunoreactivity in NM neurons at 6h following cochlea removal. **A-B:** Images of p-eEF2 immunoreactivity (A) and Y10B immunoreactivity (B) in the same section in the deprived NM at 6h following cochlea removal. Neurons with a lower intensity of p-eEF2 labeling tend to have a lower level of Y10B labeling. Arrows and arrowheads indicate neurons with high and low intensities of both labels, respectively. Dashed curves in the inserts outline the border of a lightly labeled neuron. White frames indicate the location of the insert. **C-D:** Scatter plots from a representative individual animal with unilateral cochlea removal showing integrative p-eEF2 intensity as a function of integrative Y10B intensity in intact (C) and afferent-deprived (D) NM neurons from the same section. Note a group of neurons (Box in D) with abnormally low intensities for both labels present in the deprived, but not the intact, NM. **E-F:** Scatter plots of normalized grouped data; p-eEF2 intensity as a function of normalized Y10B intensity in intact (E) or afferent-deprived (F) NM neurons. All cells were combined from multiple sections and animals. Pearson's correlation coefficient and significance are indicated for each plot. Scale bar is 25 μm in A-B and 12.5 μm in inserts.

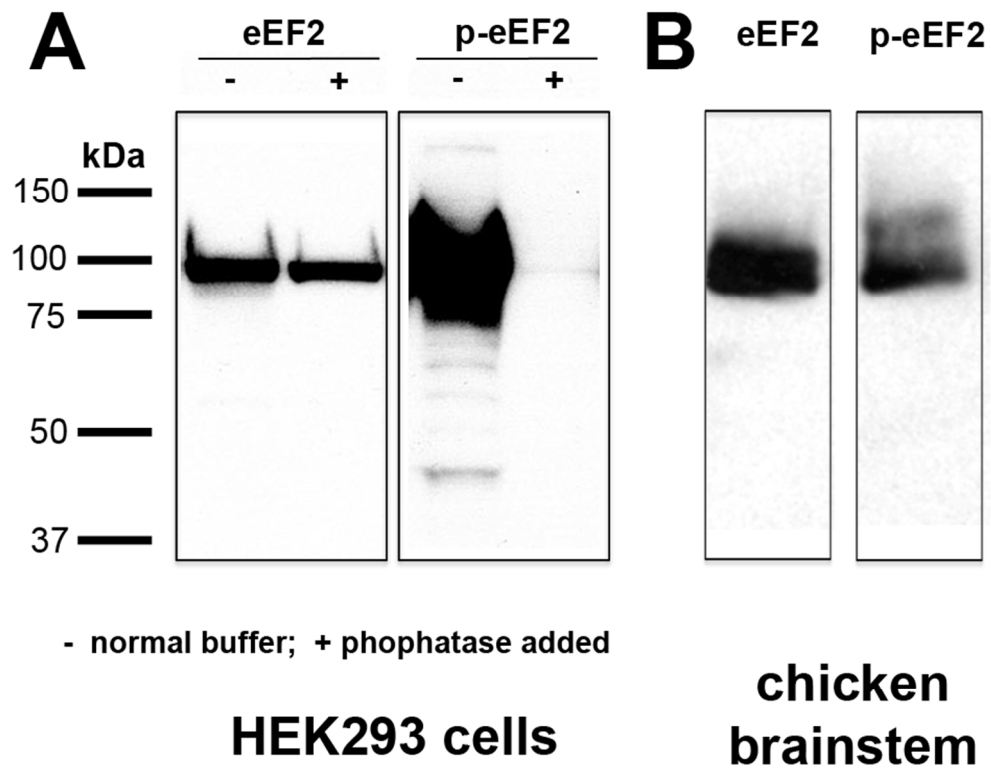

Figure 1: Western blot assay of anti-eEF2 and anti-p-eEF2 in HEK293 cells (A) and in chick dorsocaudal brainstem (B). Molecular weight standards (left) were used to determine relative sizes of labeled proteins. Anti-eEF2 detects a single band of approximately 95 kDa in both HEK293 cells and chick brainstem regardless of phosphatase treatment. Anti-p-eEF2 detects a single band of the same molecular weight in chick brainstem and HEK293 cells under normal conditions, but is absent in HEK293 cells following phosphatase treatment.
81x63mm (300 x 300 DPI)

Accepted

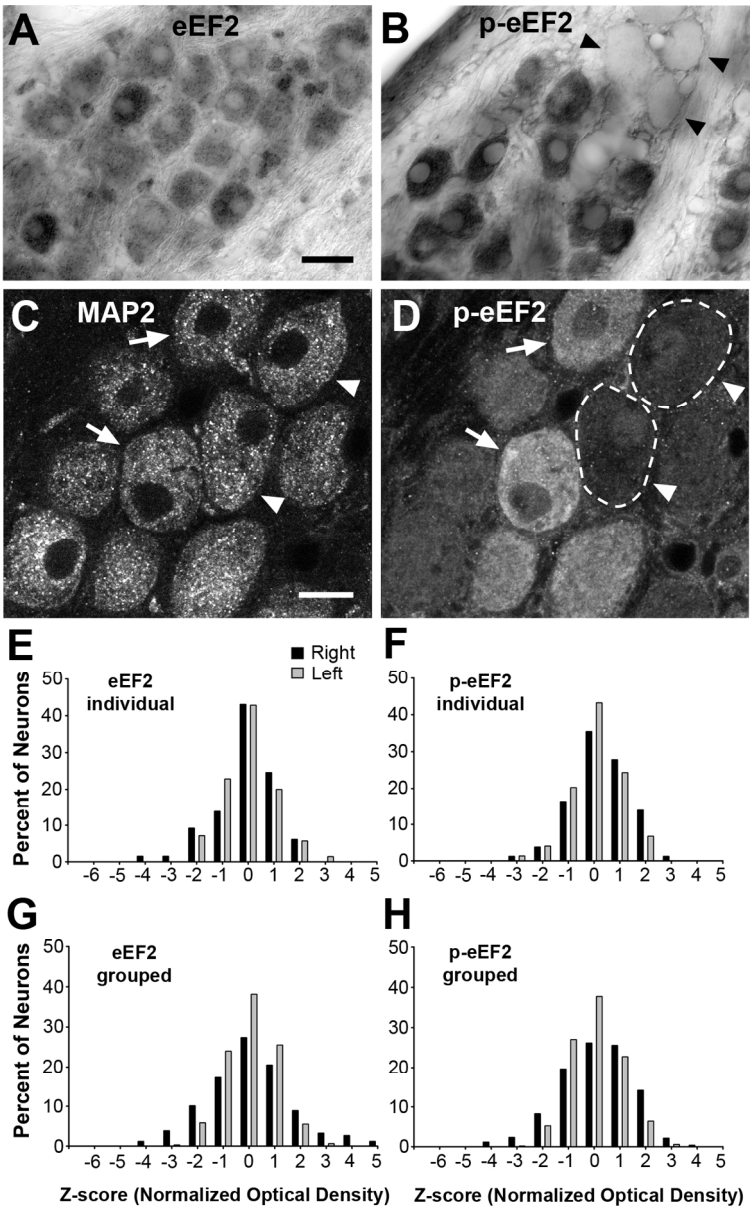

Figure 2: Immunoreactivity for eEF2 and p-eEF2 in normally innervated NM neurons. A-B: Differential interference contrast (DIC) images of NM neurons labeled by eEF2 (A) or p-eEF2 (B) immunoreactivity. Note high variability of p-eEF2 immunoreactivity across NM neurons. Arrowheads indicate a cluster of very lightly labeled neurons. Image contrast, brightness, and gamma were adjusted for optimum viewing in this and subsequent figures in Adobe Photoshop CS4. Paired sections always had identical manipulations of these properties. C-D: Fluorescent images of the same section through NM neurons double labeled for MAP2 (C) and p-eEF2 (D) immunoreactivity. Arrows indicate neurons that exhibit high levels of both MAP2 and p-eEF2, while arrowheads indicate neurons that exhibit a high level of MAP2 and a low level of p-eEF2 labeling. Dashed lines outline the border of two lightly labeled cells in D. E-F: Frequency histograms of z-scores of NM neurons labeled for eEF2 (E) or p-eEF2 (F) from an individual animal. G-H: Grouped frequency histograms of z-scores of NM neurons labeled for eEF2 (G) or p-eEF2 (H) complied from all control animals. Each neuron represents an individual data point in these histograms. For both eEF2 and p-eEF2 immunoreactivities, the distribution of z-scores is comparable between the left (grey bars) and right (black

bars) NMs. Each bar represents the total number or percentage of neurons with a z-score within ±0.5 of the assigned value of the bin, and this applies to all histograms in this and subsequent figures. Scale bar is 20 μm in A (applies for A-B) and 10 μm in C (applies for C-D).
112x180mm (300 x 300 DPI)

Accepted Article

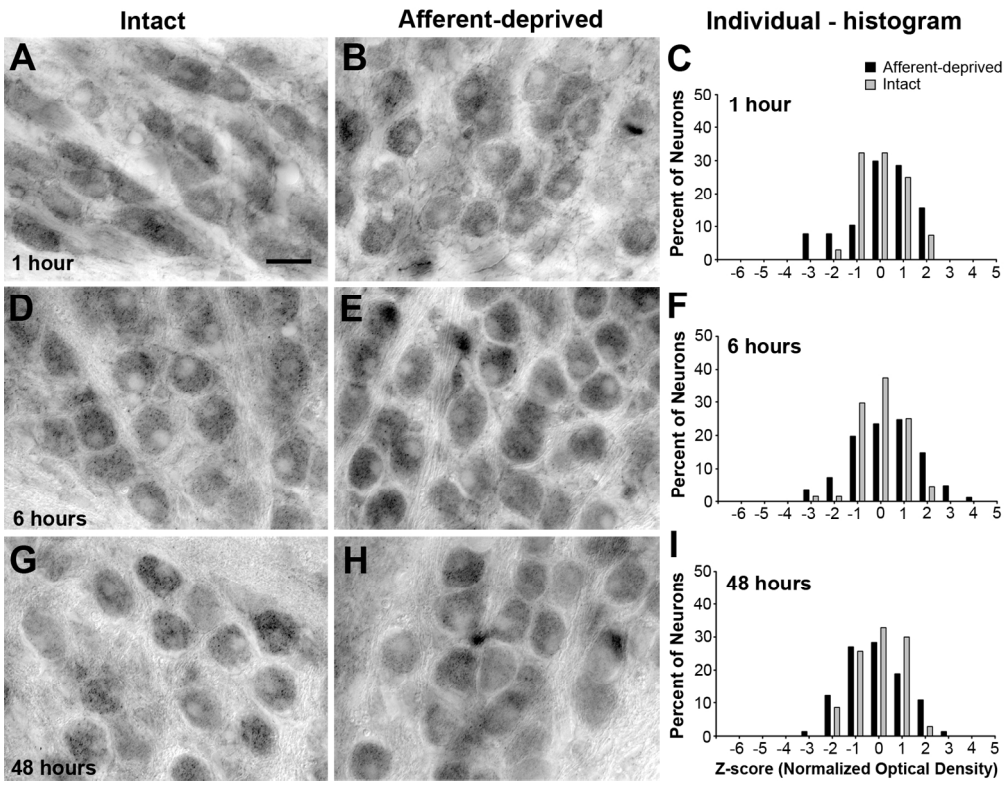

Figure 3: Time course of eEF2 immunoreactivity at 1h (A-C), 6h (D-F), and 48h (G-I) following unilateral cochlea removal. Each row represents an individual animal from a survival group and is organized from left to right in the following order: an image of the left (intact) NM (for example in the first row, A), an image of the right (deprived) NM (B), and individual frequency histograms of z-scores in both NMs (C). Each neuron represents an individual data point in these histograms. No notable difference in eEF2 immunoreactivity between the intact and deprived NMs is detected at any time points. The distribution of z-scores is comparable between the two NMs at all time points. Scale bar is 20 μm.
152x117mm (300 x 300 DPI)

Accepted

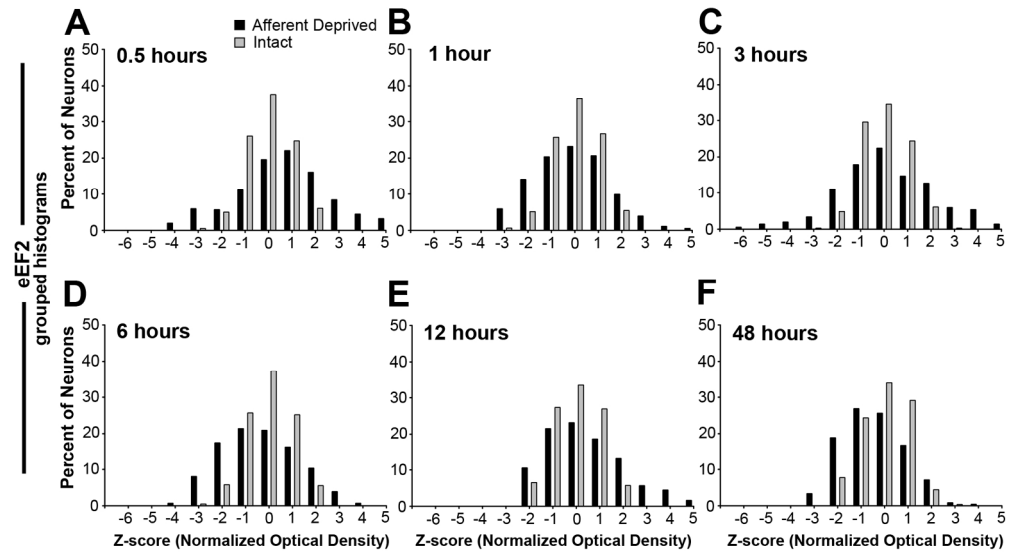

Figure 4: Grouped frequency histograms of z-scores of eEF2 immunoreactivity following unilateral cochlea removal at 0.5h (A), 1h (B), 3h (C), 6h (D), 12h (E), and 48h (F). Each neuron represents an individual data point in these histograms. Neurons from all animals within an individual survival group are complied separately for the intact (grey bars) and deprived (black bars) sides. Consistent with individual histograms illustrated in Figure 3, the distribution of z-scores is comparable between the two NMs at all time points.
171x93mm (300 x 300 DPI)

Accepted

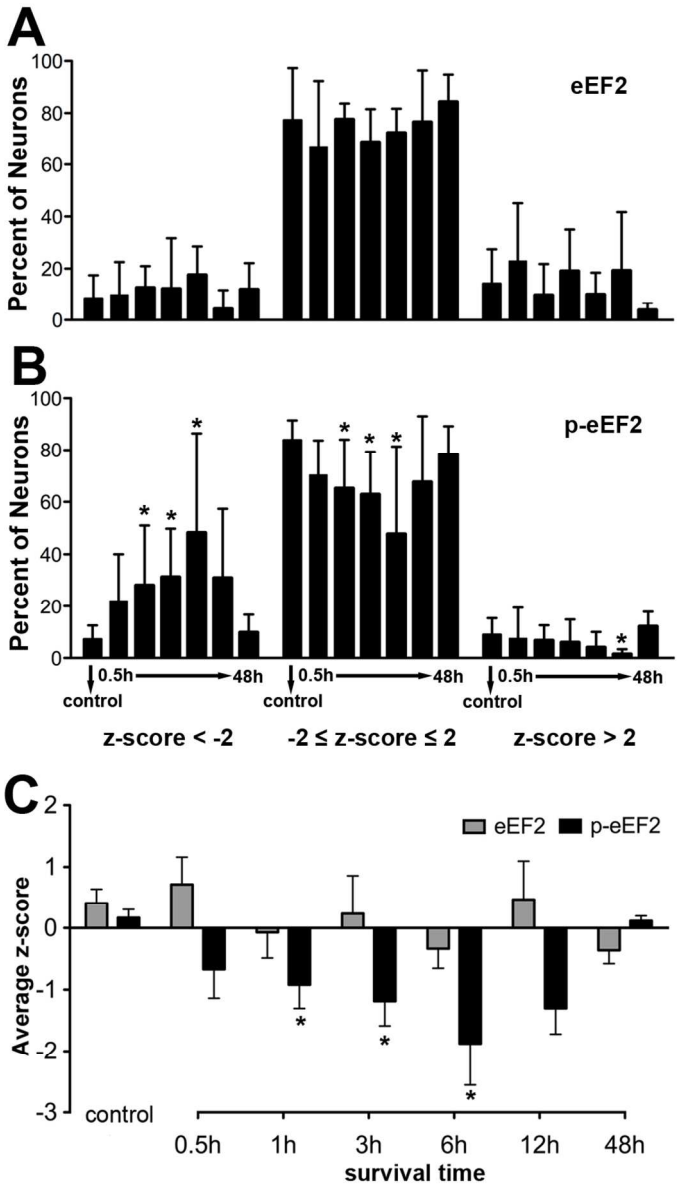

Figure 5: Analyses of changes in eEF2 and p-eEF2 immunoreactivity at the population level. Each animal represents an individual data point in these analyses; means and SEMs are presented. A-B: Percent of neurons in deprived NM with z-scores below -2 (left), between -2 and 2 (middle), and above 2 (right) for eEF2 (A) and p-eEF2 (B) immunoreactivities for each survival group. An asterisk above an individual group indicates that the percentage of neurons within each z-score range at that survival time is significantly different ($p < 0.05$) from the control group. C: Average z-score of eEF2 (grey bars) and p-eEF2 (black bars) immunoreactivity in deprived NM neurons. An asterisk above individual groups indicates that the z-score of a survival group is significantly different ($p < 0.05$) from the control group.
81x143mm (300 x 300 DPI)

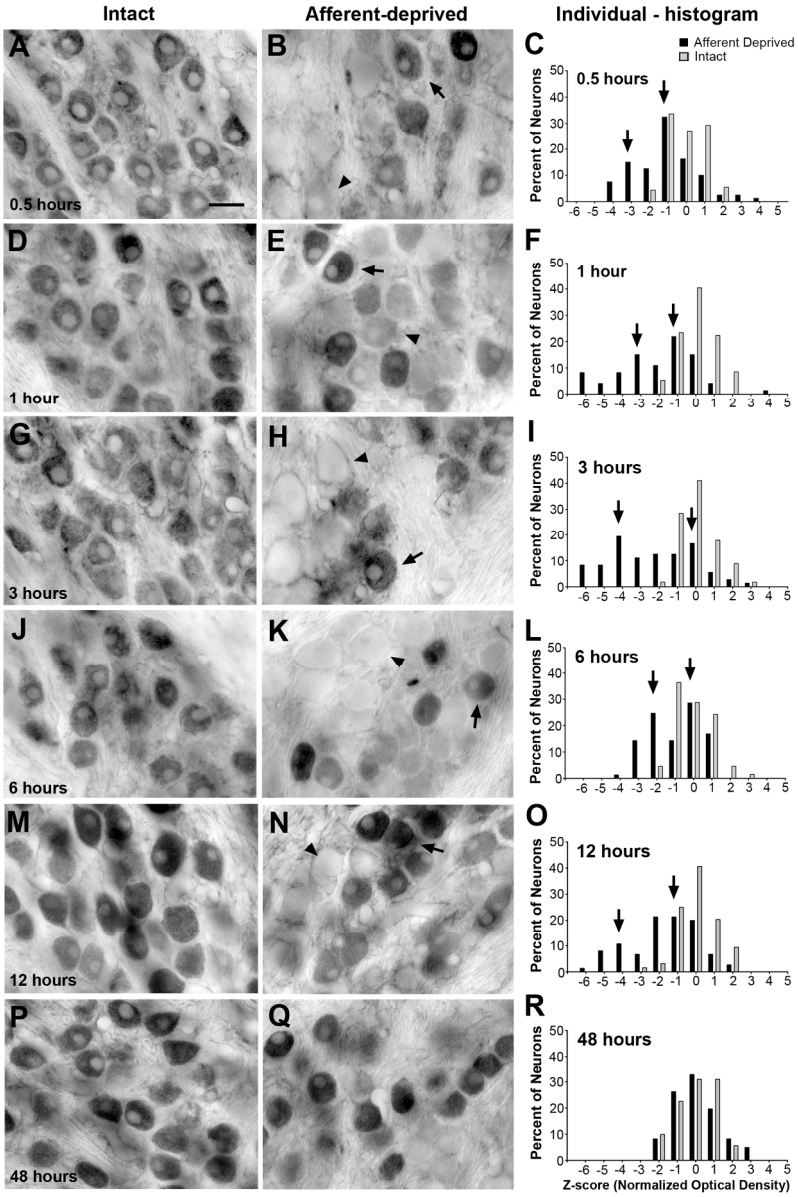

Figure 6: Time course of p-eEF2 immunoreactivity at 0.5h (A-C), 1h (D-F), 3h (G-I), 6h (J-L), 12h (M-O), and 48h (P-R) following unilateral cochlea removal. Each row represents an individual animal from a survival group and is organized from left to right in the following order: an image of the left (intact) NM (for example in the first row, A), an image of the right (deprived) NM (B), and individual frequency histograms of z-scores in both NMs (C). Each neuron represents an individual data point in these histograms. Arrows and arrowheads in the images indicate examples of darkly and lightly labeled neurons, respectively. Arrows in the histograms point out two visually detectable peaks of the z-score distribution in the deprived NM (black bars). Note not all animals exhibit two readily detected peaks. At 48h, the distribution of the immunoreactivity is comparable between two NMs. Scale bar is 20 μm.
152x230mm (300 x 300 DPI)

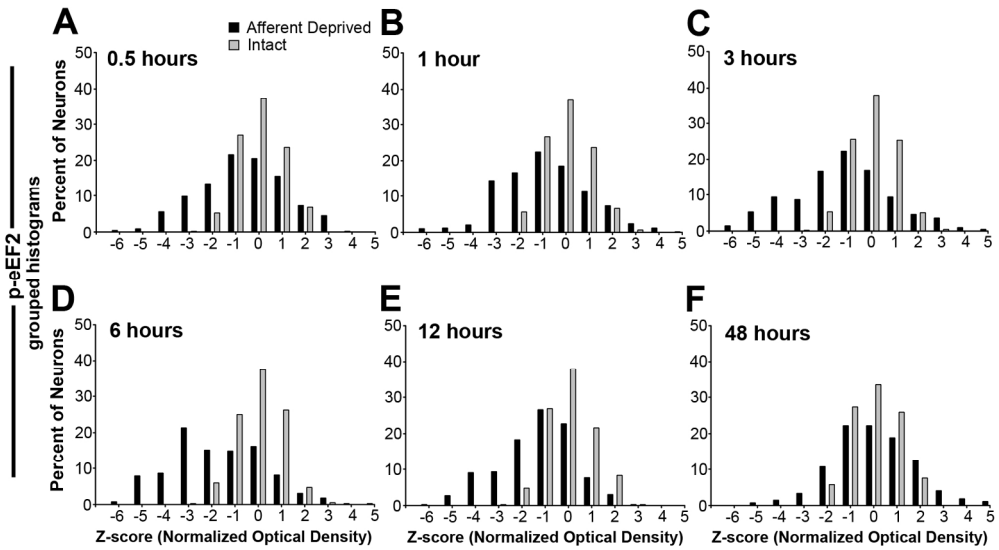

Figure 7: Grouped frequency histograms of z-scores of p-eEF2 immunoreactivity following unilateral cochlea removal at 0.5h (A), 1h (B), 3h (C), 6h (D), 12h (E), and 48h (F). Each neuron represents an individual data point in these histograms. Neurons from all animals within an individual survival group are complied separately for the intact (grey bars) and deprived (black bars) sides. Consistent with individual histograms illustrated in Figure 6, reductions in p-eEF2 immunoreactivity start at 0.5h, become more prominent between 1-6h, and disappear at 48h.
171x93mm (300 x 300 DPI)

Accepted

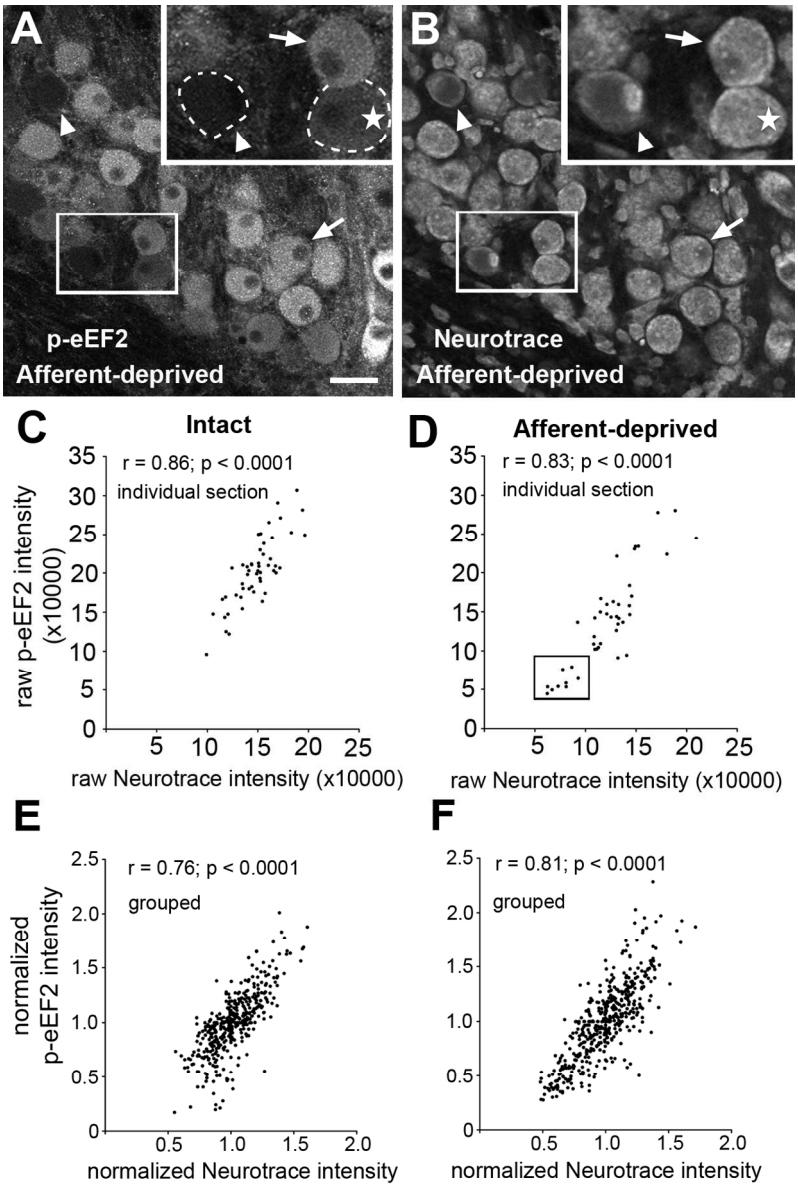

Figure 8: Correlation of p-eEF2 immunoreactivity with Neurotrace staining in NM neurons at 12h following cochlea removal. A-B: Images of p-eEF2 immunoreactivity (A) and Neurotrace labeling (B) in the same section in the deprived NM at 12h following cochlea removal. Neurons with a lower intensity of p-eEF2 labeling tend to have a lower level of Neurotrace labeling. Arrowheads indicate "ghost neurons" without reliable immunoreactivity for p-eEF2. Arrows indicate neurons with high intensities of both labels. Occasionally, neurons with a low level of p-eEF2 have a high level of Neurotrace staining (stars). Dashed lines outline the border of two lightly labeled neurons. White frames indicate the location of the insert. C-D: Scatter plots from a representative individual animal with unilateral cochlea removal showing integrative p-eEF2 intensity as a function of integrative Neurotrace intensity in intact (C) and afferent-deprived (D) NM neurons from the same section. Note a group of neurons (Box in D) with abnormally low intensities for both labels present in the deprived, but not the intact, NM. E-F: Scatter plots of normalized grouped data; p-eEF2 intensity as a function of normalized Neurotrace intensity in intact (E) or afferent-deprived (F) NM neurons. All cells were combined from multiple sections and animals. Pearson's correlation coefficient and significance are indicated for each plot. Scale bar is 25 μm in A-B and 12.5 μm in inserts.

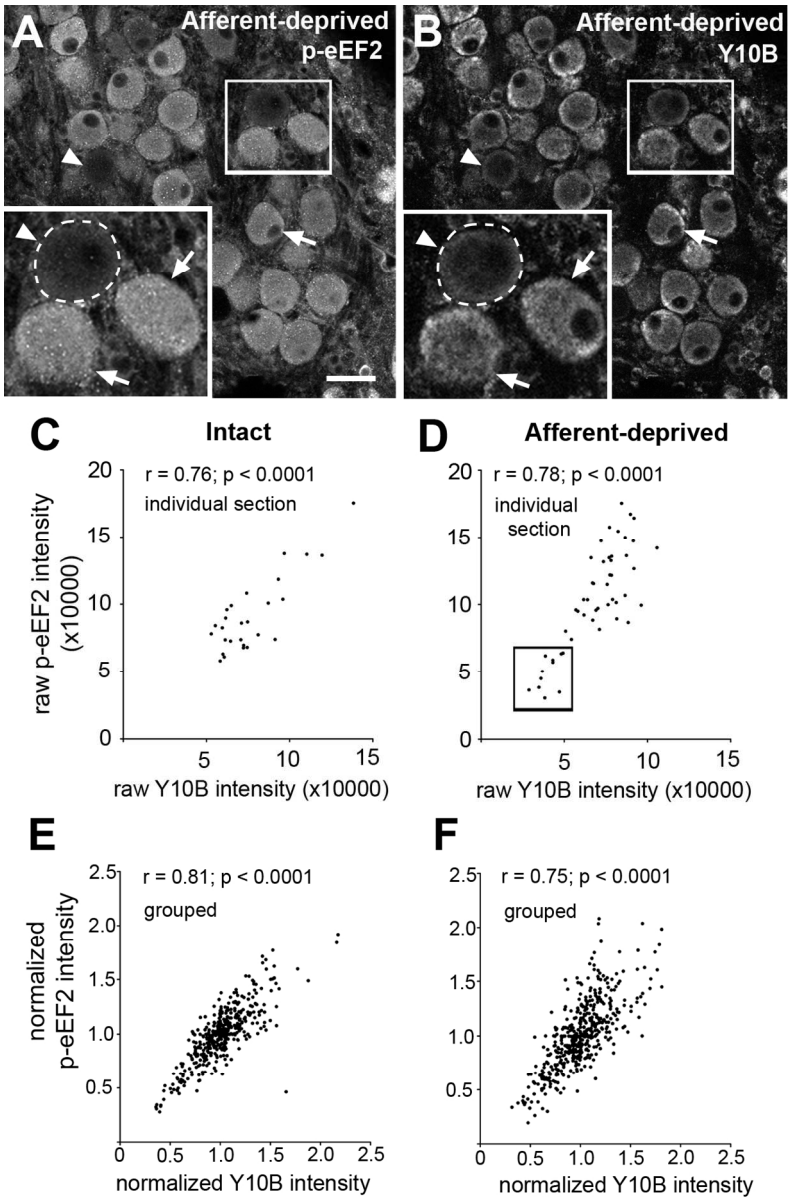

Figure 9: Correlation of p-eEF2 immunoreactivity with Y10B immunoreactivity in NM neurons at 6h following cochlea removal. A-B: Images of p-eEF2 immunoreactivity (A) and Y10B immunoreactivity (B) in the same section in the deprived NM at 6h following cochlea removal. Neurons with a lower intensity of p-eEF2 labeling tend to have a lower level of Y10B labeling. Arrows and arrowheads indicate neurons with high and low intensities of both labels, respectively. Dashed curves in the inserts outline the border of a lightly labeled neuron. White frames indicate the location of the insert. C-D: Scatter plots from a representative individual animal with unilateral cochlea removal showing integrative p-eEF2 intensity as a function of integrative Y10B intensity in intact (C) and afferent-deprived (D) NM neurons from the same section. Note a group of neurons (Box in D) with abnormally low intensities for both labels present in the deprived, but not the intact, NM. E-F: Scatter plots of normalized grouped data; p-eEF2 intensity as a function of normalized Y10B intensity in intact (E) or afferent-deprived (F) NM neurons. All cells were combined from multiple sections and animals. Pearson's correlation coefficient and significance are indicated for each plot. Scale bar is 25 μm in A-B and 12.5 μm in inserts.

Table 1: Primary antibodies used in the current study.

Name	Immunogen	Manufacturer	Species	Concentration
anti-eEF2	Synthetic peptide corresponding to residues at amino terminus of human eEF2 "FTVDQIRAIMDKKANIR"	Cell Signaling Technology (Danvers, MA), #2332	Rabbit polyclonal	1:100
anti-p-eEF2	Synthetic phosphopeptide corresponding to residues surrounding Thr56 of human eEF2. "GETRFtDTRK" The phosphor-threonine is indicated in lower case.	Cell Signaling Technology (Danvers, MA), #2331	Rabbit polyclonal	1:250
Y10B	A hybridoma was made by fusing spleen cells from a mouse model for autoimmune disease with the myeloma SP 2/0. The antibodies produced were screened and the antibody for rRNA was identified by its specificity for nucleic acid motifs common to most rRNA molecules.	Provided by Dr. Joan Steitz (Yale University)	Mouse monoclonal	1:500
anti-MAP2	Bovine brain MAP2 (aa 997-1332)	Chemicon International (Temecula, CA), # MAB3418	Mouse monoclonal	1:1000

Table 1: Primary antibodies used for the current study. The optimal primary antibody concentration was obtained by running a series of concentration tests to avoid floor or ceiling truncation, including a negative control by omitting primary antibody. Abbreviations are eukaryotic elongation factor 2 (eEF2), phosphorylated eEF2 (p-eEF2), and microtubule associated protein 2 (MAP2).

Accepted Article